Bioorganic & Medicinal Chemistry 17 (2009) 7002–7007

Contents lists available at ScienceDirect

Bioorganic & Medicinal Chemistry

journal homepage: www.elsevier.com/locate/bmc

Push–pull benzothiazole derivatives as probes for detecting β-amyloid plaques in Alzheimer's brains

Masahiro Ono [a,*,†], Shun Hayashi [a,†], Hiroyuki Kimura [a], Hidekazu Kawashima [b], Morio Nakayama [c], Hideo Saji [a,*]

[a] Graduate School of Pharmaceutical Sciences, Kyoto University, 46-29 Yoshida Shimoadachi-cho, Sakyo-ku, Kyoto 606-8501, Japan
[b] Graduate School of Medicine, Kyoto University, Shogoin Kawahara-cho, Kyoto 606-8507, Japan
[c] Graduate School of Biomedical Sciences, Nagasaki University, 1-14 Bunkyo-machi, Nagasaki 852-8521, Japan

ARTICLE INFO

Article history:
Received 29 June 2009
Revised 4 August 2009
Accepted 4 August 2009
Available online 20 August 2009

Keywords:
β-Amyloid
Push–pull dye
Imaging
Alzheimer's disease

ABSTRACT

We synthesized push–pull benzothiazole derivatives and evaluated their potential as β-amyloid imaging probes. In binding experiments in vitro, the benzothiazoles showed excellent affinity for synthetic Aβ(1-42) aggregates. β-Amyloid plaques in the mouse and human brain were clearly visualized with the benzothiazoles, reflecting the results in vitro. These compounds may be a useful scaffold for the development of novel PET/SPECT and fluorescent tracers for detecting β-amyloid in Alzheimer's brains.

1. Introduction

The formation of β-amyloid (Aβ) plaques is a key neurodegenerative event in Alzheimer's disease (AD).[1,2] Since the imaging of these plaques in vivo may lead to the presymptomatic diagnosis of AD, many molecular probes for this purpose, including PET/SPECT and MRI tracers, have been developed.[3–12] The PET ligand [^{11}C]-2-(4-(methylamino)phenyl)-6-hydroxybenzothiazole (6-OH-BTA-1 or PIB) with a benzothiazole backbone (Fig. 1) has shown particular promise in early clinical trials and is currently being used in a number of human studies.[13–15] In addition to PET/SPECT and MRI probes, much attention has focused on the development of near-infrared fluorescent (NIRF) probes targeting Aβ plaques.[16–18] NIRF probes are typically small molecule fluorescent dyes designed to absorb and emit light in the near-infrared region, where tissue scattering and absorption is lowest. The simple synthesis, low-cost, and long shelf-life of NIRF probes, together with the low-cost of optical imaging devices, present an attractive alternative to MRI and PET/SPECT techniques.

Among NIRF probes reported, to date, NIAD crosses the blood–brain barrier, selectively binds Aβ with high affinity, clears quickly from the brain, and absorbs and emits within the near-infrared region (650–900 nm), often called the 'optical window' (Fig. 1).[17] A series of NIAD derivatives have been designed and synthesized based on a classical push–pull architecture with terminal donor (hydroxy or dimethylamino group) and acceptor (dicyanomethylene group) moieties that are interconnected by a highly polarized bridge (dithienylethenyl group), because various donor and acceptor groups can be used to manipulate the relative energies of HOMO and LUMO and obtain the desired long wavelength of absorption/emission bands.[17]

On the basis of this approach to the molecular design, we planned to develop novel push–pull dyes for detecting Aβ plaques in the brain. We selected benzothiazole or styrylbenzothiazole as the highly polarized bridge, a dimethylamino group as the donor, and a dicyanomethylene group as the acceptor. In the present study, we designed and synthesized two benzothiazole-derived push–pull dyes (PP-BTA-1 and PP-BTA-2 in Fig. 2), and evaluated their biological potential as probes for detecting Aβ plaques in the brain. To our knowledge, this is the first time push–pull benzothiazole derivatives have been proposed as Aβ imaging probes for detecting AD.

2. Results and discussion

The target benzothiazole derivatives were prepared as shown in Schemes 1 and 2. PP-BTA-1 (**4**) was successfully synthesized in a yield of 21.4% according to methods reported previously (Scheme

* Corresponding authors. Tel.: +81 75 753 4608; fax: +81 75 753 4568 (M.O), tel.: +81 75 753 4556; fax: +81 75 753 4568 (H.S.).
E-mail addresses: ono@pharm.kyoto-u.ac.jp (M. Ono), hsaji@pharm.kyoto-u.ac.jp (H. Saji).
† These authors contributed equally to this work.

0968-0896/$ - see front matter © 2009 Elsevier Ltd. All rights reserved.
doi:10.1016/j.bmc.2009.08.032

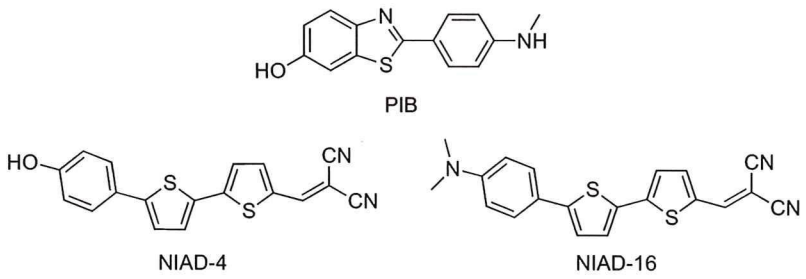

Figure 1. Chemical structures of PIB, NIAD-4 and NIAD-16.

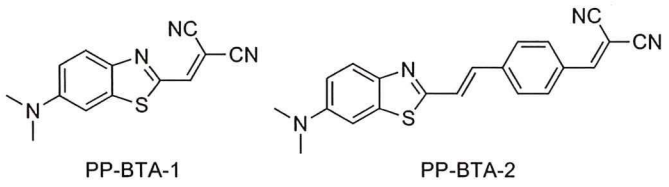

Figure 2. Chemical structures of push–pull benzothiazole derivatives reported in this paper.

1).[19] The formation of styrylbenzothiazole in the synthesis of PP-BTA-2 (**7**) (Scheme 2) was achieved by a Wadsworth–Emmons reaction between diethyl (4-cyanobenzyl)phosphonate and 6-dimethylaminobenzothiazole-2-carbaldehyde. The desired (*E*)-styrylbenzothiazole derivative was prepared in a yield of 23.0%. The cyano group was converted to a formyl group by a reaction with DIBAL-H as reported.[20] The target PP-BTA-2 was prepared by the condensation of carbaldehyde with malononitrile.

NIRF imaging in vivo requires the development of new fluorescent compounds with optimal fluorescent properties and high affinity for Aβ plaques. First, we evaluated the fluorescent properties (absorption/emission wavelengths) of PP-BTA-1 and PP-BTA-2. PP-BTA-1 and PP-BTA-2 exhibited absorption/emission peaks at 540/634 nm and 410/529 nm in EtOH, respectively. The extension of π-conjugation generally leads to absorption/emission bands with longer wavelengths. However, PP-BTA-2 showed a shorter wavelength than PP-BTA-1 despite a longer π-conjugation. On the other hand, because the wavelength of PP-BTA-1 is close to the near-infrared region, a slight modification should lead to a wavelength appropriate for imaging in vivo. Furthermore, when PP-BTA-1 and PP-BTA-2 existed in a solution containing Aβ(1-42) aggregates, the fluorescence intensity of PP-BTA-1 and PP-BTA-2 increased with the concentration of Aβ(1-42) aggregates, indicating affinity for Aβ aggregates (Fig. 3).

To quantify the affinity of push–pull benzothiazole derivatives for Aβ plaques, we carried out inhibition assays on the binding to Aβ(1-42) aggregates with thioflavin T as a competing ligand. PP-BTA-1 and PP-BTA-2 displaced thioflavin T in a dose-dependent manner, indicating that they have affinity for Aβ(1-42) aggregates (Fig. 4). In addition, this result suggests that PP-BTA-1 and PP-BTA-2 may occupy a binding site on Aβ aggregates similar to that of thioflavin T. The apparent IC_{50} values for PP-BTA-1, PP-BTA-2 and PIB were 0.12, 0.11 and 0.67 μM, respectively (Table 1). The IC_{50} of

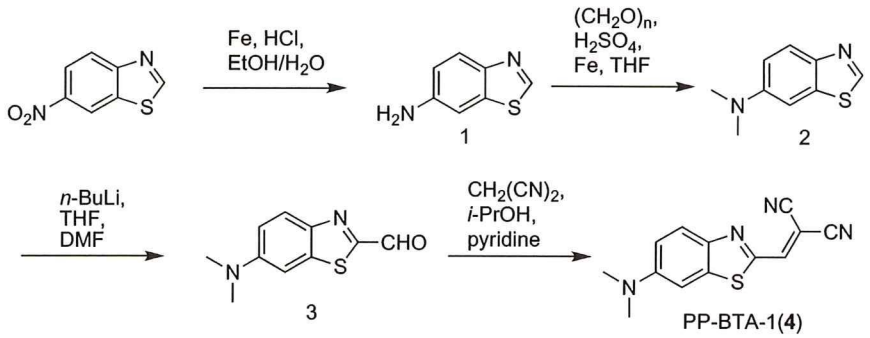

Scheme 1.

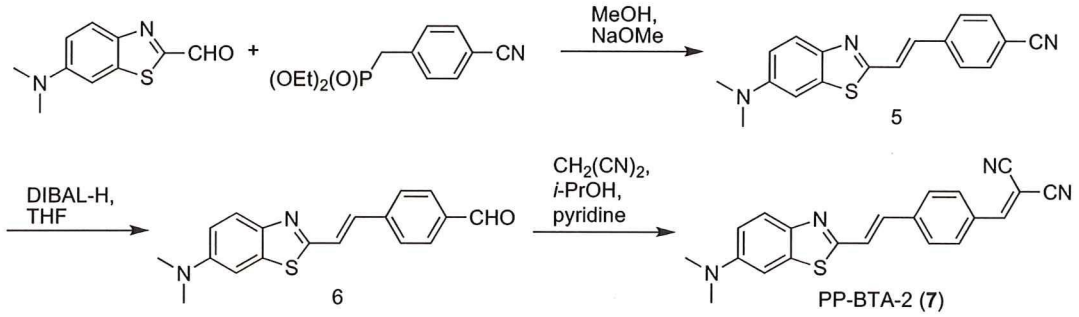

Scheme 2.

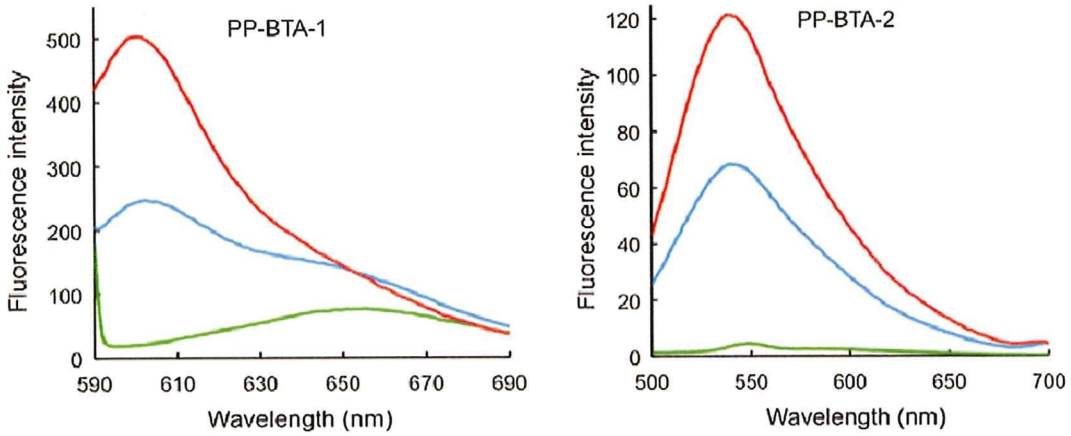

Figure 3. Aβ-dependent change in the fluorescence spectra of PP-BTA-1 and PP-BTA-2. Green, blue and red lines show the fluorescence spectrum of 0, 5 and 10 μg/mL of Aβ(1-42) aggregates, respectively.

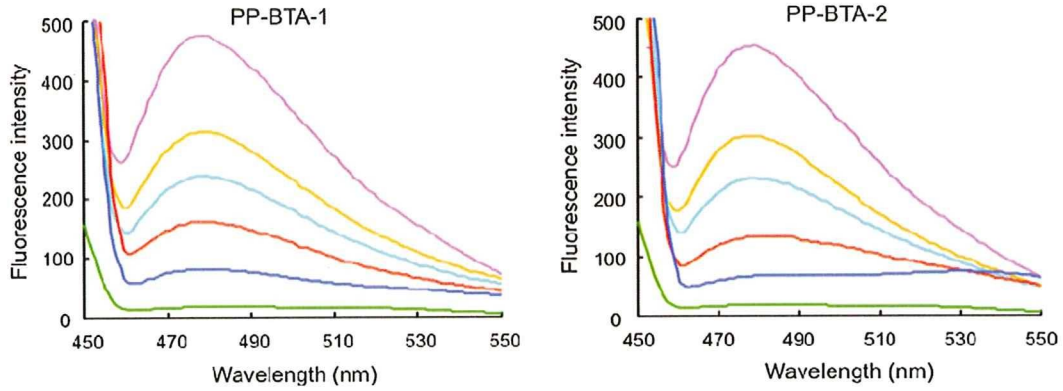

Figure 4. Inhibition assays of PP-BTA-1 and PP-BTA-2 using thioflavin T as the ligand in Aβ(1-42) aggregates. Fluorescence spectral change of thioflavin T (3 μM) upon addition of 0.0611 (orange line), 0.122 (cyan line), 0.486 (red line), or 2.65 (blue line) μM of PP-BTA-1 and PP-BTA-2 to Aβ(1-42) aggregates (10 μg/mL). A pink line shows the fluorescence spectrum of thioflavin T (3 μM) with Aβ(1-42) aggregates. A green line shows the fluorescence spectrum of thioflavin T (3 μM) alone.

Table 1
Apparent inhibition constants (IC_{50}, μM) of benzothiazoles for the binding of thioflavin T to Aβ(1-42) aggregates

Compound	IC_{50}[a] (μM)
PP-BTA-1 (**4**)	0.12 ± 0.001
PP-BTA-2 (**7**)	0.11 ± 0.001
PIB	0.67 ± 0.11

[a] Each value represents the mean ± standard error of the mean for three independent experiments.

PP-BTA-1 and PP-BTA-2 was lower than that of PIB, which is commonly used for clinical research, indicating PP-BTA-1 and PP-BTA-2 to have greater affinity for Aβ(1-42) aggregates. While PP-BTA-1 does not have the phenyl group in the phenylbenzothiazole structure that PIB possesses, it showed stronger binding to Aβ aggregates than PIB. Moreover, benzothiazole is a compact molecule advantageous for penetration of the blood–brain barrier after administration in vivo. These results suggest benzothiazole to be a useful scaffold for the development of Aβ imaging agents in vivo.

Next, the usefulness of PP-BTA-1 and PP-BTA-2 for neuropathological staining of Aβ plaques was investigated in an animal model of AD, the Tg2576 mouse, specifically engineered to overproduce Aβ plaques in the brain. PP-BTA-1 and PP-BTA-2 clearly stained the plaques as reflected by the high affinity for Aβ aggregates in in vitro competition assays (Fig. 5). The labeling pattern was consistent with that observed with thioflavin S. In contrast, wild-type mice displayed no remarkable accumulation of PP-BTA-1 and PP-BTA-2 in brain sections. These results suggest that PP-BTA-1 and PP-BTA-2 show affinity for Aβ plaques in the mouse brain in addition to having affinity for synthetic Aβ(1-42) aggregates.

Furthermore, we also investigated the effectiveness of PP-BTA-1 and PP-BTA-2 for neuropathological staining of Aβ plaques in human AD brain sections (Fig. 6). A previous report suggested the configuration/folding of Aβ plaques in Tg2576 mice to be different from the tertiary/quaternary structure of Aβ plaques in AD brains.[21] Therefore, it is important to evaluate the binding affinity for Aβ plaques in human AD brains. PP-BTA-1 and PP-BTA-2 clearly stained many neuritic plaques in AD brains (Fig. 6A and D). In contrast, no apparent staining was observed in adult normal brain sections (Fig. 6C and F). The labeling pattern was consistent with that observed by immunohistochemical labeling with an antibody specific to Aβ Fig. 6B and E), indicating that PP-BTA-1 and PP-BTA-2 may be applicable for in vivo imaging of Aβ plaques in Alzheimer's brains and deserve further investigation as a potential tool for early diagnosis.

Since PP-BTA-1 and PP-BTA-2 possess a dimethylamino group, they can be used as probes for PET by labeling one of two methyl groups with $^{11}CH_3$. In addition, for the application of push–pull benzothiazole derivatives to optical imaging in vivo, the fine-tuning of absorption/emission wavelengths to a desired region continues by optimizing the combination of donor and acceptor groups.

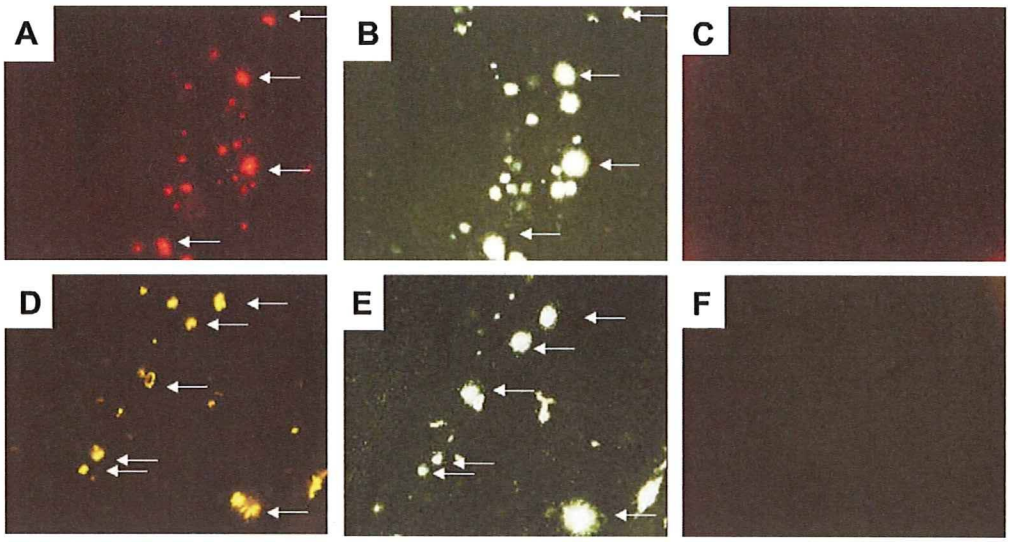

Figure 5. Neuropathological staining of PP-BTA-1 and PP-BTA-2 in 10 μm sections from a mouse model of AD (A and D) and a wild-type mouse (C and F). Aβ plaques labeled with PP-BTA-1 and PP-BTA-2 were confirmed by staining of the serial sections using thioflavin S (B and E).

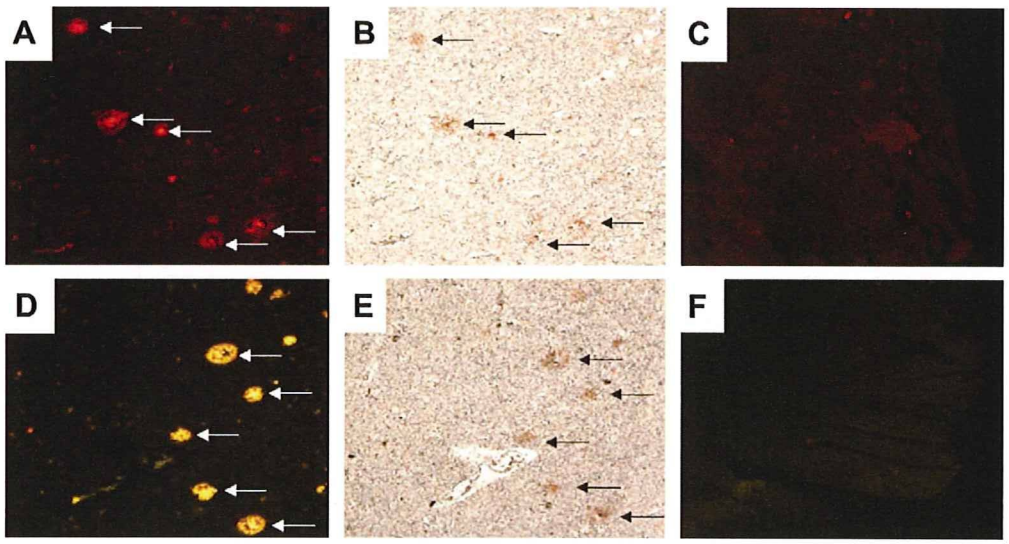

Figure 6. Neuropathological staining of 5 μm AD brain sections from the temporal cortex (A, B, D and E) and adult normal temporal brain sections (C and F). Many neuritic plaques are clearly stained with PP-BTA-1 (A) and PP-BTA-2 (D). Intense fluorescence can be seen in the core of neuritic plaques. Aβ immunostaining with anti Aβ antibodies in the serial sections shows an identical staining pattern of plaques (B and E). No apparent staining was observed in adult normal brain sections (C and F).

3. Conclusion

In conclusion, we successfully designed and synthesized benzothiazole-derived push–pull dyes for imaging Aβ plaques in the brain. In binding experiments in vitro, these benzothiazole compounds showed high affinity for Aβ(1-42) aggregates. PP-BTA-1 and PP-BTA-2 clearly stained Aβ plaques in both mouse brain and human brain, reflecting their affinity for Aβ aggregates in vitro. These findings suggest that additional structural changes on the benzothiazole backbone may be applied to potential Aβ probes for not only optical imaging but also PET and SPECT.

4. Experimental

^{1}H NMR spectra were obtained on a JEOL JNM-LM400 with TMS as an internal standard. Coupling constants are reported in hertz. Multiplicity was defined by s (singlet), d (doublet), t (triplet), br (broad) and m (multiplet). Mass spectra were obtained on a SHIMADZU LCMS-2010 EV. PIB was purchased from ABX (Radeberg, Germany). Other reagents were of reagent grade and used without further purification unless otherwise indicated.

4.1. Chemistry

4.1.1. 1,3-Benzothiazol-6-amine (1)

To a mixture of 6-nitrobenzothiazole (2.5 g, 13.9 mmol) and concentrated HCl (1.93 mL, 22.7 mmol) in 80% EtOH (63 mL) was added powdered iron (3.7 g, 55.6 mmol). The reaction mixture was stirred for 1 h under reflux, and then cooled to room temperature. The precipitate of iron oxides and hydroxy salts was removed by filtration. The solvent was removed and the solid residue was extracted into a heterogeneous mixture of EtOAc (50 mL × 2) and a 10% aqueous solution of Na_2CO_3 (50 mL). The EtOAc extract was dried (Na_2SO_4) and the solvent was removed under vacuum to yield **1** (1.91 g, 91.7%). ^{1}H NMR (400 MHz, $CDCl_3$) δ 8.70 (s, 1H), 7.89 (d, J = 8.8 Hz, 1H), 7.17 (d, J = 2.4 Hz, 1H), 6.87 (dd, J = 8.8, 2.4 Hz, 1H), 3.85 (br s, 2H). MS m/z 151 [MH^+].

4.1.2. *N,N*-Dimethyl-1,3-benzothiazol-6-amine (2)

A solution of **1** (1.47 g, 9.8 mmol) in THF (40 mL) was slowly added to a stirred mixture of 40% aqueous formaldehyde (7.24 mL, 98 mmol) and 4 M H_2SO_4 (7.95 mL, 29.4 mL). Powdered iron (4.36 g, 78.4 mL) was then added and the mixture was vigorously stirred for 3 h. The precipitate of iron salts was removed by filtration and washed with EtOAc (20 mL × 2). The combined organic solutions were made strongly basic with 1 N NaOH (50 mL) and extracted with EtOAc (50 mL × 2). The combined EtOAc extracts were dried (Na_2SO_4) and the solvent was removed on a rotary vacuum evaporator. The oily residue was purified by silica gel chromatography (hexane/EtOAc = 4:1) to give **2** (460 mg, 26.3%). ^{1}H NMR (400 MHz, $CDCl_3$) δ 8.67 (s, 1H), 7.95 (d, J = 8.8 Hz, 1H), 7.15 (d, J = 2.4 Hz, 1H), 7.00 (dd, J = 8.8, 2.4 Hz, 1H), 3.04 (s, 6H). MS m/z 179 [MH^+].

4.1.3. 6-(Dimethylamino)-1,3-benzothiazole-2-carbaldehyde (3)

To a vigorously stirred solution of *n*-BuLi (0.5 mL, 2.6 M in hexane, 1.3 mmol) in THF (5.8 mL) at −78 °C under N_2 was added slowly a solution of **2** (220 mg, 1.23 mmol). The reaction mixture was stirred, warmed to −50 °C and after 1 h cooled to −78 °C. To the resulting solution of aryllithium salt was added slowly anhydrous DMF (0.38 mL). The solution was stirred for 2 h, poured into H_2O (9 mL), neutralized with an aqueous saturated solution of NH_4Cl and subsequently extracted with EtOAc (20 mL × 2). The combined extracts were dried over Na_2SO_4 and the solvent was removed under vacuum to give **3** (255 mg, 97.3%). ^{1}H NMR (400 MHz, $CDCl_3$) δ 10.06 (s, 1H), 8.03 (d, J = 10.0 Hz, 1H), 7.07–7.04 (m, 2H), 3.12 (s, 6H). MS m/z 207 [MH^+].

4.1.4. ((6-(Dimethylamino)-1,3-benzothiazol-2-yl)methylene)-malononitrile (PP-BTA-1, 4)

A solution of **3** (124 mg, 0.6 mmol), malononitrile (60 mg, 0.9 mmol) and pyridine (0.12 mL) in 2-propanol (7.2 mL) was stirred and refluxed for 30 min. The mixture was poured into H_2O (20 mL) and extracted with $CHCl_3$ (20 mL × 3). The combined extracts were dried over Na_2SO_4 and the solvent was removed under vacuum to give **4** (152 mg, 91.7%). ^{1}H NMR (400 MHz, $CDCl_3$) δ 7.99 (s, 1H), 7.99 (d, J = 9.2 Hz, 1H), 7.08 (dd, J = 9.2, 2.4 Hz, 1H), 7.02 (d, J = 2.4 Hz, 1H), 3.16 (s, 6H). MS m/z 255 [MH^+]. Anal. Calcd for $C_{13}H_{10}N_4S$: C, 61.40; H, 3.96; N, 22.03; S, 12.61. Found: C, 61.34; H, 3.84; N, 21.82; S, 12.64.

4.1.5. 4-((*E*)-2-(6-(Dimethylamino)-1,3-benzothiazol-2-yl) vinyl)benzonitrile (5)

To a solution of (4-cyanobenzyl)phosphonate (403.6 mg, 1.6 mmol) in MeOH (12.8 mL) was added NaOMe (0.632 mL). The mixture was cooled in an ice bath, and stirred under reflux for 3 h after the addition of **3** (330 mg, 1.6 mmol). The solid that formed in the reaction mixture was filtered to give **5** (385 mg, 78.8%). ^{1}H NMR (400 MHz, $CDCl_3$) δ 7.84 (d, J = 9.6 Hz, 1H), 7.64 (dd, J = 21.2, 8.0 Hz, 4H), 7.45 (d, J = 16.4 Hz, 1H), 7.32 (d, J = 16.4 Hz, 1H), 7.06 (d, J = 2.8 Hz, 1H), 6.95 (dd, J = 9.6, 2.8 Hz, 1H), 3.06 (s, 6H). MS m/z 306 [MH^+].

4.1.6. 4-((*E*)-2-(6-(Dimethylamino)-1,3-benzothiazol-2-yl) vinyl)benzaldehyde (6)

To a solution of **5** (61 mg, 0.2 mmol) in THF (3.3 mL) was added DIBAL-H (1 M in hexane, 0.5 mL) at −78 °C. The reaction mixture was stirred at room temperature overnight. Thereafter, 10% acetic acid (15 mL) was added and the mixture was extracted with $CHCl_3$ (20 mL × 2). After the organic layer was washed with saline, the combined extracts were dried over Na_2SO_4. The residue was purified by silica gel chromatography (hexane/EtOAc = 2:1) to give **6** (28 mg, 45.4%). ^{1}H NMR (400 MHz, $CDCl_3$) δ 10.02 (s, 1H), 7.90 (d, J = 8.4 Hz, 2H), 7.85 (d, J = 8.2 Hz, 1H), 7.67 (d, J = 8.4 Hz, 2H), 7.50 (d, J = 16.4 Hz, 1H), 7.38 (d, J = 16.4 Hz, 1H), 7.07 (d, J = 2.4 Hz, 1H), 6.96 (dd, J = 8.8, 2.4 Hz, 1H), 3.06 (s, 6H). MS m/z 309 [MH^+].

4.1.7. 4-((*E*)-2-(6-(Dimethylamino)-1,3-benzothiazol-2-yl) vinyl)benzylidene)malononitrile (PP-BTA-2, 7)

The same reaction as described above to prepare **5** was used, and 45 mg of **7** was obtained in a 63.5% yield from **6**. ^{1}H NMR (400 MHz, $CDCl_3$) δ 7.94 (d, J = 8.4 Hz, 2H), 7.86 (d, J = 8.8 Hz, 1H), 7.73 (s, 1H), 7.68 (d, J = 8.4 Hz, 2H), 7.53 (d, J = 16.4 Hz, 1H), 7.35 (d, J = 16.4 Hz, 1H), 7.08 (s, 1H), 6.97 (d, J = 10.0 Hz , 1H), 3.08 (s, 6H). MS m/z 357 [MH^+]. Anal. Calcd for $C_{21}H_{16}N_4S$: C, 70.76; H, 4.52; N, 15.72; S, 9.00. Found: C, 70.48; H, 4.57; N, 15.43; S, 8.99.

4.2. Fluorescence experiments

PP-BTA-1 and PP-BTA-2 were dissolved in 5% EtOH at 10 μM. The fluorescence of PP-BTA-1 and PP-BTA-2 was measured with a spectrophotometer (RF-1500, Shimadzu, Japan). For some measurements, the spectra of PP-BTA-1 and PP-BTA-2 were determined with or without Aβ(1-42) aggregates (0, 5 and 10 μM).

4.3. Binding experiments using Aβ(1-42) aggregates

A solid form of Aβ(1-42) was purchased from Peptide Institute (Osaka, Japan). Aggregation was carried out by gently dissolving the peptide (0.25 mg/mL) in a buffer solution (pH 7.4) containing 10 mM sodium phosphate and 1 mM EDTA. The solution was incubated at 37 °C for 42 h with gentle and constant shaking. Thioflavin-T was used as the tracer for the competition binding experiments. A mixture (3.6 mL of 10% EtOH) containing PP-BTA-1, PP-BTA-2 and PIB (final concn 61.1 nM–5.48 μM), thioflavin-T (final concn 3 μM), and Aβ(1-42) aggregates (final concn 10 μg/mL) was incubated at room temperature for 10 min. Fluorescence intensity at an excitation wavelength of 445 nm was plotted, and values for the apparent half-maximal inhibitory concentration (IC_{50}) were determined from a calibration curve of fluorescence intensity at 478 nm in three independent experiments.

4.4. Staining of Aβ plaques in Tg2576 mouse brain sections

The experiments with animals were conducted in accordance with our institutional guidelines and approved by the Kyoto University Animal Care Committee. The Tg2576 transgenic mice (female, 27-month-old) and wild-type mice (female, 27-month-old) were used as the Alzheimer's model and control mice, respectively. After the mice were sacrificed by decapitation, the brains were immediately removed and frozen in powdered dry ice. The frozen blocks were sliced into serial sections, 10 μm thick. Each slide was incubated with a 50% EtOH solution (100 μM) of PP-BTA-1 and PP-BTA-2 for 10 min. The sections were washed in 50% EtOH for 1 min two times, and examined using a microscope (Nikon Eclipse 80i) equipped with a G-2A filter set (excitation, 510–560 nm; diachronic mirror, 575 nm; longpass filter, 470 nm) for PP-BTA-1, and a B-2A filter set (excitation, 450–480 nm; diachronic mirror, 505 nm; longpass filter, 520 nm) for PP-BTA-2. Thereafter, the serial sections were also stained with thioflavin S, a pathological dye commonly used for staining Aβ plaques in the brain, and examined using a microscope (Nikon Eclipse 80i) equipped with a BV-2A filter set (excitation, 400–440 nm; diachronic mirror, 455 nm; longpass filter, 470 nm).

4.5. Staining of Aβ plaques in human AD brain sections

Postmortem brain tissues from an autopsy-confirmed case of AD (73-year-old male) and a control subject (36-year-old male) were

obtained from BioChain Institute Inc. The sections were incubated with PP-BTA-1 and PP-BTA-2 (50% EtOH, 100 μM) for 10 min at room temperature. The sections were washed in 50% EtOH for 1 min two times, and examined using a microscope (Nikon Eclipse 80i) equipped with a G-2A filter set (excitation, 510–560 nm; diachronic mirror, 575 nm; longpass filter, 470 nm) for PP-BTA-1, and a B-2A filter set (excitation, 450–480 nm; diachronic mirror, 505 nm; longpass filter, 520 nm) for PP-BTA-2. The presence and localization of plaques on the same sections were confirmed with immunohistochemical staining using a monoclonal Aβ antibody, BC05 (Wako).

Acknowledgements

This study was supported by the Program for Promotion of Fundamental Studies in Health Sciences of the National Institute of Biomedical Innovation (NIBIO), a Health Labour Sciences Research Grant, and a Grant-in-Aid for Young Scientists (A) and Exploratory Research from the Ministry of Education, Culture, Sports, Science and Technology, Japan.

References and notes

1. Klunk, W. E. *Neurobiol. Aging* **1998**, *19*, 145.
2. Selkoe, D. J. *Physiol. Rev.* **2001**, *81*, 741.
3. Shoghi-Jadid, K.; Small, G. W.; Agdeppa, E. D.; Kepe, V.; Ercoli, L. M.; Siddarth, P.; Read, S.; Satyamurthy, N.; Petric, A.; Huang, S. C.; Barrio, J. R. *Am. J. Geriatr. Psychiat.* **2002**, *10*, 24.
4. Mathis, C. A.; Wang, Y.; Holt, D. P.; Huang, G. F.; Debnath, M. L.; Klunk, W. E. *J. Med. Chem.* **2003**, *46*, 2740.
5. Ono, M.; Wilson, A.; Nobrega, J.; Westaway, D.; Verhoeff, P.; Zhuang, Z. P.; Kung, M. P.; Kung, H. F. *Nucl. Med. Biol.* **2003**, *30*, 565.
6. Klunk, W. E.; Engler, H.; Nordberg, A.; Wang, Y.; Blomqvist, G.; Holt, D. P.; Bergstrom, M.; Savitcheva, I.; Huang, G. F.; Estrada, S.; Ausen, B.; Debnath, M. L.; Barletta, J.; Price, J. C.; Sandell, J.; Lopresti, B. J.; Wall, A.; Koivisto, P.; Antoni, G.; Mathis, C. A.; Langstrom, B. *Ann. Neurol.* **2004**, *55*, 306.
7. Verhoeff, N. P.; Wilson, A. A.; Takeshita, S.; Trop, L.; Hussey, D.; Singh, K.; Kung, H. F.; Kung, M. P.; Houle, S. *Am. J. Geriatr. Psychiat.* **2004**, *12*, 584.
8. Small, G. W.; Kepe, V.; Ercoli, L. M.; Siddarth, P.; Bookheimer, S. Y.; Miller, K. J.; Lavretsky, H.; Burggren, A. C.; Cole, G. M.; Vinters, H. V.; Thompson, P. M.; Huang, S. C.; Satyamurthy, N.; Phelps, M. E.; Barrio, J. R. *N. Eng. J. Med.* **2006**, *355*, 2652.
9. Kudo, Y.; Okamura, N.; Furumoto, S.; Tashiro, M.; Furukawa, K.; Maruyama, M.; Itoh, M.; Iwata, R.; Yanai, K.; Arai, H. *J. Nucl. Med.* **2007**, *48*, 553.
10. Rowe, C. C.; Ackerman, U.; Browne, W.; Mulligan, R.; Pike, K. L.; O'Keefe, G.; Tochon-Danguy, H.; Chan, G.; Berlangieri, S. U.; Jones, G.; Dickinson-Rowe, K. L.; Kung, H. P.; Zhang, W.; Kung, M. P.; Skovronsky, D.; Dyrks, T.; Holl, G.; Krause, S.; Friebe, M.; Lehman, L.; Lindemann, S.; Dinkelborg, L. M.; Masters, C. L.; Villemagne, V. L. *Lancet. Neurol.* **2008**, *7*, 129.
11. Higuchi, M.; Iwata, N.; Matsuba, Y.; Sato, K.; Sasamoto, K.; Saido, T. C. *Nat. Neurosci.* **2005**, *8*, 527.
12. Poduslo, J. F.; Curran, G. L.; Peterson, J. A.; McCormick, D. J.; Fauq, A. H.; Khan, M. A.; Wengenack, T. M. *Biochemistry* **2004**, *43*, 6064.
13. Bacskai, B. J.; Frosch, M. P.; Freeman, S. H.; Raymond, S. B.; Augustinack, J. C.; Johnson, K. A.; Irizarry, M. C.; Klunk, W. E.; Mathis, C. A.; Dekosky, S. T.; Greenberg, S. M.; Hyman, B. T.; Growdon, J. H. *Arch. Neurol.* **2007**, *64*, 431.
14. Johnson, K. A.; Gregas, M.; Becker, J. A.; Kinnecom, C.; Salat, D. H.; Moran, E. K.; Smith, E. E.; Rosand, J.; Rentz, D. M.; Klunk, W. E.; Mathis, C. A.; Price, J. C.; Dekosky, S. T.; Fischman, A. J.; Greenberg, S. M. *Ann. Neurol.* **2007**, *62*, 229.
15. Pike, K. E.; Savage, G.; Villemagne, V. L.; Ng, S.; Moss, S. A.; Maruff, P.; Mathis, C. A.; Klunk, W. E.; Masters, C. L.; Rowe, C. C. *Brain* **2007**, *130*, 2837.
16. Hintersteiner, M.; Enz, A.; Frey, P.; Jaton, A. L.; Kinzy, W.; Kneuer, R.; Neumann, U.; Rudin, M.; Staufenbiel, M.; Stoeckli, M.; Wiederhold, K. H.; Gremlich, H. U. *Nat. Biotechnol.* **2005**, *23*, 577.
17. Nesterov, E. E.; Skoch, J.; Hyman, B. T.; Klunk, W. E.; Bacskai, B. J.; Swager, T. M. *Angew. Chem., Int. Ed. Engl.* **2005**, *44*, 5452.
18. Raymond, S. B.; Skoch, J.; Hills, I. D.; Nesterov, E. E.; Swager, T. M.; Bacskai, B. J. *Eur. J. Nucl. Med. Mol. Imaging* **2008**, *35*, S93.
19. Hrobarik, P.; Sigmundova, I.; Zahradnik, P. *Synthesis* **2005**, *4*, 600.
20. Cho, B. R.; Chajara, K.; Jung, H.; Son, K. H.; Jeon, S. J. *Org. Lett.* **2002**, *4*, 1703.
21. Toyama, H.; Ye, D.; Ichise, M.; Liow, J. S.; Cai, L.; Jacobowitz, D.; Musachio, J. L.; Hong, J.; Crescenzo, M.; Tipre, D.; Lu, J. Q.; Zoghbi, S.; Vines, D. C.; Seidel, J.; Katada, K.; Green, M. V.; Pike, V. W.; Cohen, R. M.; Innis, R. B. *Eur. J. Nucl. Med. Mol. Imaging* **2005**, *32*, 593.

6394 J. Med. Chem. 2009, 52, 6394–6401
DOI: 10.1021/jm901057p

Journal of
Medicinal
Chemistry
Article

Fluoro-pegylated Chalcones as Positron Emission Tomography Probes for in Vivo Imaging of β-Amyloid Plaques in Alzheimer's Disease

Masahiro Ono,*[,†,‡] Rumi Watanabe,[†] Hidekazu Kawashima,[§] Yan Cheng,[‡] Hiroyuki Kimura,[‡] Hiroyuki Watanabe,[†] Mamoru Haratake,[†] Hideo Saji,[‡] and Morio Nakayama*[,†]

[†]*Department of Hygienic Chemistry, Graduate School of Biomedical Sciences, Nagasaki University, 1-14 Bunkyo-machi, Nagasaki 852-8521, Japan,* [‡]*Department of Patho-Functional Bioanalysis, Graduate School of Pharmaceutical Sciences, Kyoto University, Yoshida Shimoadachi-cho, Sakyo-ku, Kyoto 606-8501, Japan, and* [§]*Department of Nuclear Medicine and Diagnostic Imaging, Graduate School of Medicine, Kyoto University, Shogoin Kawahara-cho, Sakyo-ku, Kyoto 606-8507, Japan*

Received July 16, 2009

This paper describes the synthesis and biological evaluation of fluoro-pegylated (FPEG) chalcones for the imaging of β-amyloid (Aβ) plaques in patients with Alzheimer's disease (AD). FPEG chalcone derivatives were prepared by the aldol condensation reaction. In binding experiments conducted in vitro using Aβ(1−42) aggregates, the FPEG chalcone derivatives having a dimethylamino group showed higher K_i values (20−50 nM) than those having a monomethylamino or a primary amine group. When the biodistribution of ^{11}C-labeled FPEG chalcone derivatives having a dimethyamino group was examined in normal mice, all four derivatives were found to display sufficient uptake for imaging Aβ plaques in the brain. ^{18}F-labeled **7c** also showed good uptake by and clearance from the brain, although a slight difference between the ^{11}C and ^{18}F tracers was observed. When the labeling of Aβ plaques was carried out using brain sections of AD model mice and an AD patient, the FPEG chalcone derivative **7c** intensely labeled Aβ plaques. Taken together, the results suggest **7c** to be a useful candidate PET tracer for detecting Aβ plaques in the brain of patients with AD.

Introduction

The formation of β-amyloid (Aβ[a]) plaques is a key neurodegenerative event in Alzheimer's disease (AD).[1,2] Because the imaging of Aβ plaques in vivo may lead to the presymptomatic diagnosis of AD, many radiotracers that bind to Aβ plaques have been developed.[3,4] Preliminary reports of positron emission tomography (PET) suggested that the uptake and retention of 2-(4′-[^{11}C]methylaminophenyl)-6-hydroxybenzothiazole ([^{11}C]PIB, **1**)[5,6] and 4-*N*-[^{11}C]methylamino-4′-hydroxystilbene ([^{11}C]SB-13, **2**)[7,8] differed between the brain of AD patients and those of controls. However, because ^{11}C is a positron-emitting isotope with a $t_{1/2}$ of just 20 min, efforts are being made to develop comparable agents labeled with the isotope ^{18}F ($t_{1/2}$ = 110 min). [^{18}F]-2-(1-(2-(*N*-(2-fluoroethyl)-*N*-methylamino)-naphthalene-6-yl)ethylidene)malononitrile ([^{18}F]FDDNP, **3**)[9,10] and [^{18}F]-4-(*N*-methylamino)-4′-(2-(2-(2-fluoroethoxy)ethoxy)-stilbene ([^{18}F]BAY94−9172, **4**)[11,12] should be useful as tracers for imaging Aβ plaques in the diagnosis of AD. Recent reports suggest that Aβ aggregates possess multiple ligand-binding sites, the density of which differs.[13−15] Therefore, the development of novel probes that bind Aβ aggregates may lead to critical findings regarding the pathology of AD.

Recently, in a search for novel Aβ-imaging probes, we found that radioiodinated flavone,[16,17] chalcone,[18,19] and aurone[20,21] derivatives, which are categorized as flavonoids, showed excellent characteristics such as high affinity for Aβ aggregates and good uptake into and rapid clearance from the brain. The chalcone structure in particular is considered to be a useful core in the development of new Aβ-imaging probes because it can be formed by a one-pot condensation reaction. In addition, because chalcone derivatives show different characteristics of binding to Aβ aggregates from Congo Red and thioflavin T, they are expected to provide new information from in vivo imaging in AD brains.

In the present study, we designed and synthesized fluorinated chalcone derivatives for the purpose of developing ^{18}F-labeled probes for PET-based imaging of Aβ plaques. The formation of bioconjugates based on pegylation-fluorination resulting in fluoro-pegylated (FPEG) molecules is effective for some core structures of Aβ-imaging probes.[22] We have adopted a novel approach, adding a short PEG (n = 1−3) to the chalcone backbone and capping the end of the ethylene glycol chain with a fluorine atom. Indeed, the most promising ^{18}F-labeled agent **4** possesses PEG (n = 3) in the stilbene backbone. This tracer showed strong affinity (K_i = 6.7 nM) for Aβ plaques, high uptake (7.77%ID/g at 2 min postinjection), and rapid clearance from the mouse brain

*To whom correspondence should be addressed. For M.O.: phone, +81-75-753-4608; fax, +81-75-753-4568; E-mail, ono@pharm.kyoto-u.ac.jp. For M.N.: phone, +81-95-819-2441; fax, +81-95-819-2441; E-mail: morio@nagasaki-u.ac.jp.

[a]Abbreviations: Aβ, β-amyloid; AD, Alzheimer's disease; PET, positron emission tomography; PIB, 2-(4′-methyaminophenyl)-6-hydroxybenzothiazole; SB-13, 4-*N*-methylamino-4′-hydroxystilbene; FDDNP, 2-(1-(2-(*N*-(2-fluoroethyl)-*N*-methylamino)naphthalene-6-yl)ethylidene)-malononitrile; BAY94-9174, 4-(*N*-methylamino)-4′-(2-(2-(2-fluoroethoxy)ethoxy)ethoxy)-stilbene; DMIC, 4-dimethylamino-4′-iodo-chalcone; IMPY, 6-iodo-2-(4′-dimethylamino)phenyl-imidazo[1,2-*a*]pyridine; FPEG, fluoro-pegylated; DAST, diethylamino sulfur trifluoride; DME, 1,2-dimethoxyethane; MEK, methyl ethyl ketone; [^{11}C]methyl triflate, [^{11}C]MeOTf; DAB, 3,3′-diaminobenzidine.

 Published on Web 09/16/2009

Scheme 1

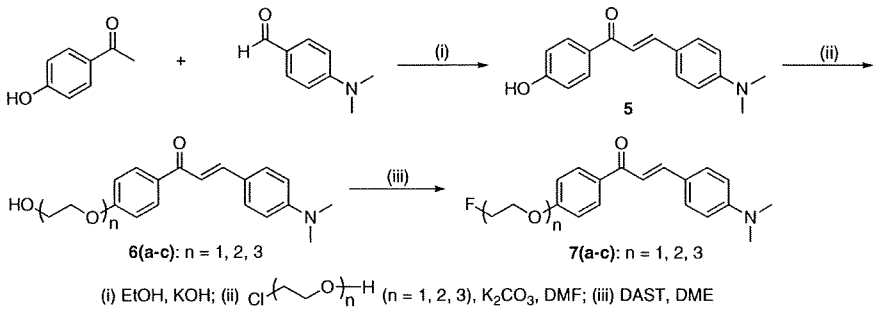

Scheme 2

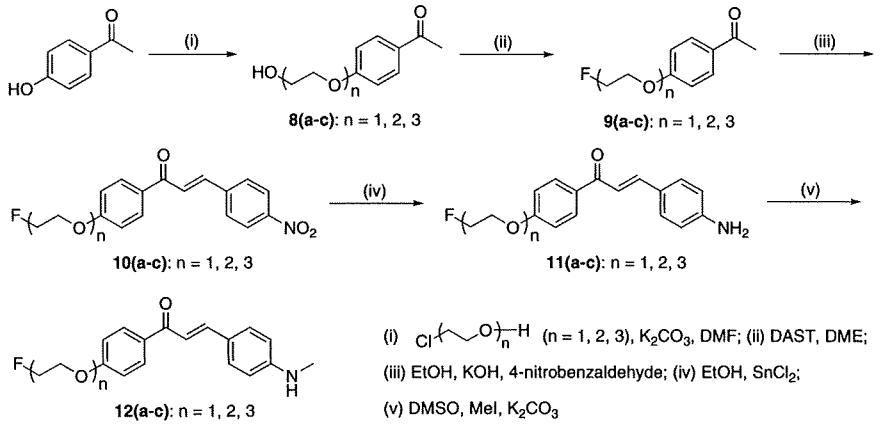

Scheme 3[a]

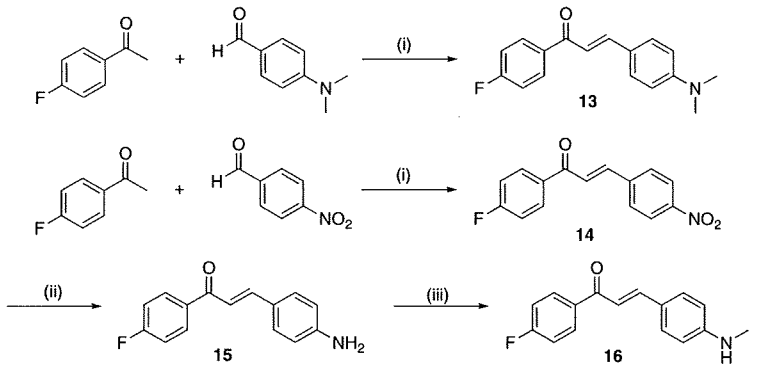

[a] (i) EtOH, KOH; (ii) EtOH, $SnCl_2$; (iii) DMSO, MeI, K_2CO_3.

(1.61%ID/g at 60 min postinjection).[12] We adopted the biological data for **4** as criteria to develop novel Aβ-imaging agents. In this study, we synthesized 12 fluorinated chalcones and evaluated their biological potential as Aβ-imaging agents by testing their affinity for Aβ aggregates and Aβ plaques in sections of brain tissue from AD model mice and an AD patient and their uptake by and clearance from the brain in biodistribution experiments using normal mice.

Results and Discussion

The synthesis of the FPEG chalcone derivatives is outlined in Schemes 1, 2, and 3. The most useful way to prepare chalcones is the condensation of acetophenones with ben zaldehydes. Using this process, 4-hydroxyacetophenone or 4-fluoroacetophenone was reacted with 4-dimethylaldehyde to form 4′-hydroxy-4-dimethylamino-chalcone **5** and 4′-fluoro-4-dimethylamino-chalcone **13** in yields of 84.0 and 41.6%, respectively. Compounds **10(a−c)** were synthesized by an aldol reaction between FPEG acetophenone **9(a−c)** and 4-nitrobenzaldehyde. Fluorination of **6(a−c)** and **8(a−c)** to prepare **7(a−c)** and **9(a−c)** was done using diethylamino sulfur trifluoride (DAST) after introducing three oligoethylene glycol molecules into the phenolic OH of **5** and **9(a−c)**. The amino derivatives **11(a−c)** and **15** were readily prepared from **10(a−c)** and **14** by reduction with $SnCl_2$. Conversion of **11(a−c)** and **15** to the monomethylamino derivatives **12(a−c)** and **16** was achieved by methylation with CH_3I under alkaline conditions. Preparation of ^{11}C-labeled compounds was done as in Scheme 4. ^{11}C-labeled chalcones

Scheme 4

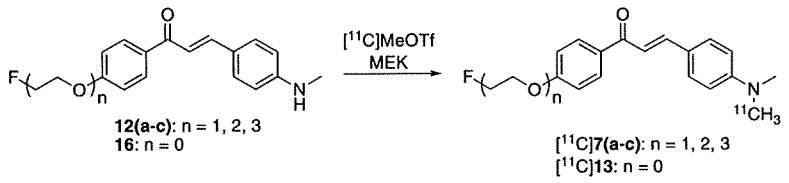

Scheme 5

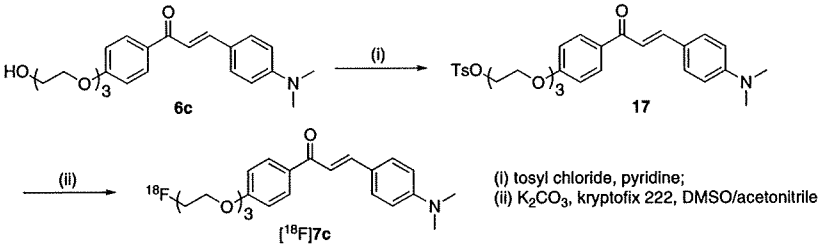

Table 1. Chemical Structures and Inhibition Constants of Fluorinated Chalcone Derivatives

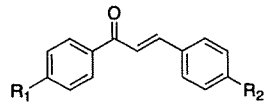

compd	R_1	R_2	K_i (nM)[a]
7a	FCH_2CH_2O	$N(CH_3)_2$	45.7 ± 7.1
7b	$F(CH_2CH_2O)_2$	$N(CH_3)_2$	20.0 ± 2.5
7c	$F(CH_2CH_2O)_3$	$N(CH_3)_2$	38.9 ± 4.2
11a	FCH_2CH_2O	NH_2	678.9 ± 21.7
11b	$F(CH_2CH_2O)_2$	NH_2	1048.0 ± 114.3
11c	$F(CH_2CH_2O)_3$	NH_2	790.0 ± 132.1
12a	FCH_2CH_2O	$NHCH_3$	197.1 ± 58.8
12b	$F(CH_2CH_2O)_2$	$NHCH_3$	216.4 ± 13.8
12c	$F(CH_2CH_2O)_3$	$NHCH_3$	470.9 ± 100.4
13	F	$N(CH_3)_2$	49.8 ± 6.2
15	F	NH_2	663.0 ± 88.3
16	F	$NHCH_3$	234.2 ± 44.0
DMIC	I	$N(CH_3)_2$	13.1 ± 3.0
IMPY			28.0 ± 4.1

[a] Inhibition constants (K_i, nM) of compounds for the binding of [^{125}I]DMIC to Aβ(1−42) aggregates. Values are the mean ± standard error of the mean for 4−9 independent experiments.

were readily synthesized from their *N*-normethyl precursors, **12(a−c)** and **16**, and [^{11}C]methyl triflate ([^{11}C]-MeOTf). Radiochemical yields of the final product were 28−35%, decay corrected to end of bombardment. Radiochemical purity was >99% with a specific activity of 22−28 GBq/μmol. The identity of [^{11}C]**7a**, [^{11}C]**7b**, [^{11}C]**7c**, and [^{11}C]**13** was confirmed by a comparison of HPLC retention times with the nonradioactive compounds (**7a**, **7b**, **7c**, and **13**). ^{18}F labeling of **7c** was performed on a tosyl precursor **17** undergoing a nucleophilic displacement reaction with the fluoride anion (Scheme 5). Radiolabeling with ^{18}F was successfully performed on the precursor to generate [^{18}F]**7c** with a radiochemical yield of 45% and radiochemical purity >99%. The identity of [^{18}F]**7c** was verified by a comparison of retention time with the nonradioactive compound. The specific activity of [^{18}F]**7c** was estimated to be 35 GBq/mmol at the end of synthesis.

Table 2. Biodistribution of Radioactivity after Injection of [^{11}C]**7a**, [^{11}C]**7b**, [^{11}C]**7c**, and [^{11}C]**13** in Normal Mice[a]

organ	2 min	10 min	30 min	60 min
		[^{11}C]**7a**		
blood	3.65 ± 0.37	2.73 ± 0.28	2.12 ± 0.18	2.22 ± 0.25
brain	6.01 ± 0.61	3.24 ± 0.39	2.57 ± 0.26	2.26 ± 0.41
		[^{11}C]**7b**		
blood	3.48 ± 0.56	2.28 ± 0.84	2.54 ± 0.96	1.44 ± 0.36
brain	4.73 ± 0.47	2.23 ± 0.18	1.14 ± 0.12	1.00 ± 0.19
		[^{11}C]**7c**		
blood	2.44 ± 0.25	1.52 ± 0.42	1.01 ± 0.15	0.68 ± 0.10
brain	4.31 ± 0.33	1.38 ± 0.16	0.64 ± 0.07	0.35 ± 0.03
		[^{11}C]**13**		
blood	2.61 ± 0.35	1.60 ± 0.25	0.39 ± 0.05	1.40 ± 0.20
brain	3.68 ± 0.35	1.53 ± 0.14	1.04 ± 0.15	1.04 ± 0.20

[a] Expressed as % of injected dose per gram. Each value represents the mean ± SD for 4−5 mice.

Table 3. Biodistribution of Radioactivity after Injection of [^{18}F]**7c** in Normal Mice[a]

organ	2 min	10 min	30 min	60 min
blood	2.09 ± 0.40	1.94 ± 0.18	2.35 ± 0.33	1.87 ± 0.26
brain	3.48 ± 0.47	1.52 ± 0.03	1.08 ± 0.09	1.07 ± 0.17
bone	1.80 ± 0.31	1.76 ± 0.15	2.98 ± 0.49	3.58 ± 0.41

[a] Expressed as % of injected dose per gram. Each value represents the mean ± SD for 4−5 mice.

Experiments in vitro to evaluate the affinity of the FPEG chalcones for Aβ aggregates were carried out in solutions of Aβ aggregates with [^{125}I]4-dimethylamino-4′-iodo-chalcone ([^{125}I]DMIC)[18] as the ligand (Table 1). The K_i values suggested that the binding to Aβ(1−42) aggregates was affected by substitution at the amino group at position 4 in the chalcone structure, not by the length of PEG introduced into the chalcone backbone. The fluorinated chalcones had binding affinity for Aβ(1−42) aggregates in the following order: the dimethyamino derivatives (**7a**, **7b**, **7c**, and **13**) > the monomethylamino derivatives (**12a**, **12b**, **12c**, and **16**) > the primary amino derivatives (**11a**, **11b**, **11c**, and **15**). The result of the binding experiments is consistent with that of previous reports.[16,19] In addition, the affinity of the dimethylamino

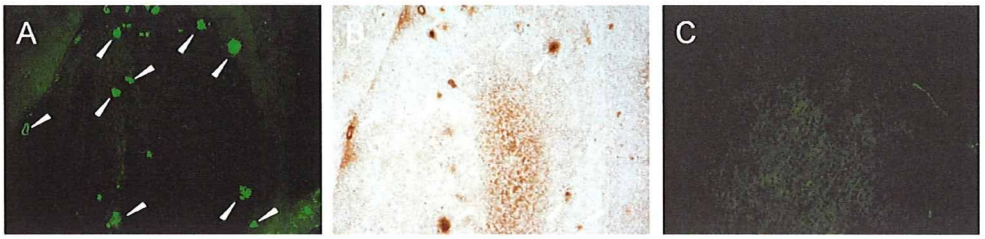

Figure 1. Neuropathological staining of 10 μm sections of a Tg2576 mouse brain (A and B) and aged normal brain (C). Fluorescent staining of compound **7c** in the Tg2576 mouse brain (A). Aβ immunostaining with antibody BC05 in the adjacent section (B). Fluorescent staining of compound **7c** in the age-matched control mouse brain (C).

derivatives was in the same range as that of the known compound, 6-iodo-2-(4′-dimethylamino)phenyl-imidazo[1,2-*a*]pyridine (IMPY), which is commonly used for inhibition assays.[22−25] We selected the dimethylamino derivatives (**7a**, **7b**, **7c**, and **13**), which showed the greatest affinity, for additional studies.

To evaluate brain uptake of the FPEG chalcones, biodistribution experiments were performed in normal mice with four ^{11}C-labeled FPEG chalcones ([^{11}C]**7a**, [^{11}C]**7b**, [^{11}C]**7c**, and [^{11}C]**13**) (Table 2). Because normal mice were used for the biodistribution experiments, no Aβ plaques were expected in the young mice; therefore the washout of probes from the brain should be rapid to obtain a higher signal-to-noise ratio earlier in the AD brain. Radioactivity after injection of the ^{11}C-labeled FPEG chalcones penetrated the blood−brain barrier, showing excellent uptake ranging from 3.7 to 6.0% ID/g brain at 2 min postinjection, a level sufficient for imaging Aβ plaques in the brain. In addition, they displayed good clearance from the normal brain with 2.3, 1.0, 0.35, and 1.0% ID/g at 60 min postinjection for [^{11}C]**7a**, [^{11}C]**7b**, [^{11}C]**7c**, and [^{11}C]**13**, respectively. These values were equal to 37.6, 21.1, 8.1, and 28.3% of the initial uptake peak for [^{11}C]**7a**, [^{11}C]**7b**, [^{11}C]**7c**, and [^{11}C]**13**, respectively. Compound **7c** with the fastest washout from the brain was labeled with ^{18}F and evaluated for its biodistribution in normal mice (Table 3). [^{18}F]**7c** displayed high uptake (3.48%ID/g) at 2 min postinjection, a level sufficient for imaging like [^{11}C]**7c**, and was cleared over the subsequent 10, 30, and 60 min. The radioactivity in the brain at 60 min postinjection was 1.07%ID/g, indicating that this [^{18}F]**7c** has favorable pharmacokinetics in the brain. Although we consider that a slight difference of the radioactivity pharmacokinetics between [^{11}C]**7c** and [^{18}F]**7c** could be attributable to the different physicochemical characteristics of their radiometabolites produced in the brain, the reason for this difference has remained unclear. Bone uptake at 60 min was measurable (3.58%ID/g), suggesting defluorination in vivo. Bone uptake has been observed for other ^{18}F tracers.[12,22−24] However, previous reports suggested that free fluoride was not taken up by brain tissue; therefore, the interference from free fluoride may be relatively low for brain imaging. A previous paper regarding the most promising ^{18}F-labeled agent **4** reported that it showed high uptake (7.77% ID/g at 2 min postinjection) and rapid clearance from the brain (1.61%ID/g at 60 min postinjection) with little accumulation in bone (1.77%ID/g at 60 min postinjection) in biodistribution experiments using normal mice.[12] The pharmacokinetics of **4** appear superior to that of [^{18}F]**7c**, but the good biological results obtained with [^{18}F]**7c** suggest that further investigation is warranted.

To investigate the ability of the fluorinated chalcones to bind to Aβ plaques in the AD model, fluorescent staining of sections of mouse brain were carried out with compound **7c** (Figure 1). We used Tg2576 transgenic mice as an animal model of Aβ plaque deposition, which express human APP695 with the K670N, M671L Swedish double mutation.[26] By 11−13 months of age, Tg2576 mice show prominent Aβ deposition in the cingulated cortex, entorhinal cortex, dentate gyrus, and CA1 hippocampal subfield and have been frequently used for the evaluation of specific binding of Aβ plaques in in vitro and in vivo experiments.[12,24,27−31] Many Aβ plaques were clearly stained with **7c**, as reflected by the affinity for the aggregates of synthetic Aβ(1−42) in in vitro competition assays (Figure 1A). The labeling pattern was consistent with that observed after immunohistochemical labeling by BC05, a specific antibody for Aβ (Figure 1B), while wild-type mouse brain displayed no significant accumulation of **7c** (Figure 1C). The results indicated that **7c** binds specifically to Aβ plaques in Tg2576 mice brain. A previous report suggested the configuration/folding of Aβ plaques in Tg2576 mice to be different from the tertiary/quaternary structure of Aβ plaques in AD brains.[30,32] In addition, the studies reported with **1** further indicate that the binding of **1** reflects the amount of Aβ plaques in human AD brain but not in Tg2576 mouse brain, and the detectability of Aβ plaques by **1** is dependent on the accumulation of specific Aβ subtypes.[28,29] Therefore, we considered that it should be essential to evaluate the binding affinity for Aβ plaques in human AD brains because our goal is to develop clinically useful probes for in vivo imaging of Aβ plaques in humans.

Next, we investigated the binding affinity of [^{18}F]**7c** for Aβ plaques by in vitro autoradiography in a human AD brain section (Figure 2A). The autoradiographic image of [^{18}F]**7c** showed high levels of radioactivity in some specific areas of the brain section. Furthermore, we confirmed that the hot spots of [^{18}F]**7c** in an AD brain section corresponded with those of in vitro thioflavin-S staining in the same brain section (Figure 2B). In contrast, no significant accumulation of [^{18}F]**7c** was observed in the region without Aβ plaques (Figure 2C). The results demonstrate the feasibility of using [^{18}F]**7c** as a probe for detecting Aβ plaques in the brain of AD patients with PET.

In conclusion, we reported novel FPEG chalcone derivatives, containing an end-capped fluoropolyethylene glycol as in vivo PET imaging agents for Aβ plaques in the brain. The FPEG chalcones with a dimethylamino group displayed greater affinity for synthetic Aβ aggregates than did the monomethylamino and primary amino derivatives. In biodistribution experiments using normal mice, ^{11}C-labeled FPEG chalcones displayed sufficient uptake for the imaging of Aβ plaques in the brain. [^{11}C]**7c** showed the fastest clearance from the brain, probably related to a low nonspecific binding. [^{18}F]**7c** also displayed high uptake in and good clearance from

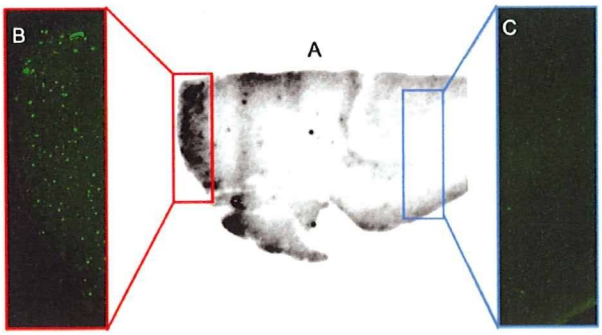

Figure 2. In vitro autoradiography of [^{18}F]**7c** using the human AD brain section (A). Aβ plaques were confirmed by in vitro staining of the same section with thioflavin-S (B and C).

the brain, although a slight difference was observed between the ^{11}C and ^{18}F tracers. When the labeling of plaques in vitro was carried out using sections of brain tissue from an animal model of AD and an AD patient, compound **7c** intensely labeled Aβ plaques existing in both brains. Taken together, the results suggest the novel FPEG chalcone **7c** to be potentially useful for imaging Aβ plaques in the brain using PET.

Experimental Section

General. All reagents were obtained commercially and used without further purification unless otherwise indicated. ^{1}H NMR spectra were obtained on a Varian Gemini 300 spectrometer with TMS as an internal standard. Coupling constants are reported in hertz. Multiplicity was defined by s (singlet), d (doublet), t (triplet) and m (multiplet). Mass spectra were obtained on a JEOL IMS-DX instrument. HPLC analysis was performed on a Shimadzu HPLC system (a LC-10AT pump with a SPD-10A UV detector, $\lambda = 254$ nm) using a Cosmosil C_{18} column (Nakalai Tesque, 5C_{18}-AR-II, 4.6 mm × 150 mm) using acetonitrile/water (50/50) as mobile phase at a flow rate of 1.0 mL/min. All key compounds were proven by this method to show ≥95% purity.

Chemistry. (*E*)-3-(4-(Dimethylamino)phenyl)-1-(4-hydroxyphenyl)-2-propen-1-one (5). 4-Hydroxyacetophenone (1.36 g, 10 mmol) and 4-dimethylaminobenzaldehyde (1.86 g, 10.0 mmol were dissolved in EtOH (15 mL). A 30 mL aliquot of a 10% aqueous KOH solution was then slowly added dropwise to the reaction mixture. The mixture was stirred for 24 h at 100 °C and then extracted with ethyl acetate. After the organic layers were combined and dried over Na_2SO_4, evaporation of the solvent afforded 1.50 g of **5** (84.0%). ^{1}H NMR (CD_3OD) δ: 3.04 (s, 6H), 6.76 (d, $J = 8.7$ Hz, 2H), 6.88 (d, $J = 8.7$ Hz, 2H), 7.50 (d, $J = 15.3$ Hz, 1H), 7.59 (d, $J = 9.0$ Hz, 2H), 7.72 (d, $J = 15.3$ Hz, 1H), 7.98 (d, $J = 8.7$ Hz, 2H). ^{1}H NMR (DMSO-d_6) δ: 2.99 (s, 6H), 6.74 (d, $J = 8.7$ Hz, 2H), 6.88 (d, $J = 8.4$ Hz, 2H), 7.62 (s, 2H), 7.68 (d, $J = 8.7$ Hz, 2H), 8.03 (d, $J = 8.7$ Hz, 2H), 10.30 (s, 1H). EI-MS: m/z 267 (M^+).

(*E*)-3-(4-(Dimethylamino)phenyl)-1-(4-(2-hydroxyethoxy)phenyl)-2-propen-1-one (6a). To a solution of **5** (500 mg, 1.87 mmol and ethylene chlorohydrin (125 μL, 1.87 mmol) in DMSO (5 mL) was added anhydrous K_2CO_3 (775 mg, 5.61 mmol). The reaction mixture was stirred for 18 h at 100 °C and then poured into water and extracted with chloroform. The organic layers were combined and dried over Na_2SO_4. Evaporation of the solvent afforded a residue, which was purified by silica gel chromatography (hexane: ethyl acetate = 1:1) to give 422 mg of **6a** (72.7%). ^{1}H NMR ($CDCl_3$) δ: 3.04 (s, 6H), 4.00−4.01 (m, 2H), 4.17 (t, $J = 4.8$ Hz, 2H), 6.69 (d, $J = 9.0$ Hz, 2H), 6.99 (d, $J = 6.9$ Hz, 2H), 7.35 (d, $J = 15.3$ Hz, 1H), 7.55 (d, $J = 9.0$ Hz, 2H), 7.79 (d, $J = 15.3$ Hz, 1H), 8.02 (d, $J = 9.3$ Hz, 2H).

(*E*)-3-(4-(Dimethylamino)phenyl)-1-(4-(2-(hydroxyethoxy)ethoxy)-phenyl)-2-propen-1-one (6b). The reaction described above to prepare **6a** was used, and **6b** was obtained from **5** and ethylene glycol mono-2-chloroethyl ether. ^{1}H NMR ($CDCl_3$) δ: 3.05 (s, 6H), 3.69 (t, $J = 4.8$ Hz, 2H), 3.78 (s, 2H), 3.91 (t, $J = 4.8$ Hz, 2H), 4.23 (t, $J = 4.8$ Hz, 2H), 6.70 (d, $J = 9.0$ Hz, 2H), 6.99 (d, $J = 9.0$ Hz, 2H), 7.35 (d, $J = 15.3$ Hz, 1H), 7.55 (d, $J = 8.7$ Hz, 2H), 7.79 (d, $J = 15.6$ Hz, 1H), 8.02 (d, $J = 9.0$ Hz, 2H).

(*E*)-3-(4-(Dimethylamino)phenyl)-1-(4-(2-((hydroxyethoxy)ethoxy)-ethoxy)phenyl)-2-propen-1-one (6c). The reaction described above to prepare **6a** was used, and 429 mg of **6c** was obtained in a yield of 82.6% from **5** and 2-[2-(2-chloroethoxy)-ethoxy]ethanol. ^{1}H NMR ($CDCl_3$) δ: 3.04 (s, 6H), 3.62 (t, $J = 5.1$ Hz, 2H), 3.73−3.75 (m, 6H), 3.90 (t, $J = 4.8$ Hz, 2H), 4.22 (t, $J = 4.8$ Hz, 2H), 6.70 (d, $J = 9.0$ Hz, 2H), 6.99 (d, $J = 8.7$ Hz, 2H), 7.35 (d, $J = 15.3$ Hz, 1H), 7.55 (d, $J = 9.0$ Hz, 2H), 7.78 (d, $J = 15.3$ Hz, 1H), 8.02 (d, $J = 9.0$ Hz, 2H).

(*E*)-3-(4-(Dimethylamino)phenyl)-1-(4-(2-fluoroethoxy)phenyl)-2-propen-1-one (7a). To a solution of **6a** (100 mg, 0.32 mmol in 1,2-dimethoxyethane (DME) (5 mL) was added DAST (85 μL, 0.64 mmol) in a dry ice−acetone bath. The reaction mixture was stirred for 1 h at room temperature and then poured into a saturated $NaHSO_3$ solution and extracted with chloroform. After the organic phase was separated, dried over Na_2SO_4, and filtered, and the residue was purified by preparative TLC (hexane:ethyl acetate = 3:1) to give 39 mg of **7a** (38.9%). ^{1}H NMR ($CDCl_3$) δ: 3.09 (s, 6H), 4.30 (d, t, $J_1 = 27.6$ Hz, $J_2 = 4.2$ Hz, 2H), 4.79 (d, t, $J_1 = 47.4$ Hz, $J_2 = 4.2$ Hz, 2H), 6.70 (d, $J = 8.7$ Hz, 2H), 7.00 (d, $J = 9.0$ Hz, 2H), 7.35 (d, $J = 15.6$ Hz, 1H), 7.55 (d, $J = 9.0$ Hz, 2H), 7.79 (d, $J = 15.3$ Hz, 1H), 8.03 (d, $J = 9.0$ Hz, 2H). EI-MS: m/z 313 (M^+).

(*E*)-3-(4-(Dimethylamino)phenyl)-1-(4-(2-(fluoroethoxy)ethoxy)-phenyl)-2-propen-1-one (7b). The reaction described above to prepare **7a** was used, and 28 mg of **7b** was obtained in a yield of 28.0% from **6b**. ^{1}H NMR ($CDCl_3$) δ: 3.04 (s, 6H), 3.77−3.94 (m, 4H), 4.21−4.24 (m, 3H), 4.61 (d, t, $J_1 = 47.4$ Hz, $J_2 = 4.2$ Hz 1H), 6.69 (d, $J = 9.3$ Hz, 2H), 6.99 (d, $J = 8.7$ Hz, 2H), 7.35 (d, $J = 15.3$ Hz, 2H), 7.55 (d, $J = 9.0$ Hz, 2H), 7.78 (d, $J = 15.6$ Hz, 2H), 8.02 (d, $J = 9.0$ Hz, 2H). EI-MS: m/z 357 (M^+).

(*E*)-3-(4-(Dimethylamino)phenyl)-1-(4-(2-((fluoroethoxy)ethoxy)-ethoxy)phenyl)-2-propen-1-one (7c). The reaction described above to prepare **7a** was used, and 29 mg of **7c** was obtained in a yield of 14.4% from **6c** and 2-[2-(2-chloroethoxy)ethoxy]ethanol. ^{1}H NMR ($CDCl_3$) δ: 3.04 (s, 6H), 3.73−3.81 (m, 6H), 3.90 (t, $J = 5.1$ Hz, 2H), 4.21 (t, $J = 5.1$ Hz, 2H), 4.49 (t, $J = 4.5$ Hz, 1H), 4.65 (t, $J = 4.5$ Hz, 1H), 6.70 (d, $J = 8.7$ Hz, 2H), 6.98 (d, $J = 9.0$ Hz, 2H), 7.35 (d, $J = 15.3$ Hz, 1H), 7.55 (d, $J = 8.7$ Hz, 2H), 7.78 (d, $J = 15.3$ Hz, 1H), 8.02 (d, $J = 9.0$ Hz, 2H). EI-MS: m/z 401 (M^+).

1-(4-(2-Hydroxyethoxy)phenyl)ethanone (8a). The reaction described above to prepare **6a** was used, and 1.79 g of **8a** was obtained in a yield of 99.4% from 4-hydroxyacetophenone and ethylene chlorohydrin. ^{1}H NMR ($CDCl_3$) δ: 2.75 (s, 3H), 4.20 (s, 2H), 4.35 (t, $J = 5.1$ Hz, 2H), 7.15 (d, $J = 9.0$ Hz, 2H), 8.13 (d, $J = 9.0$ Hz, 2H).

1-(4-(2-(2-Hydroxyethoxy)ethoxy)phenyl)ethanone (8b). The reaction described above to prepare **6b** was used, and **8b** was obtained from 4-hydroxyacetophenone and ethylene glycol mono-2-chloroethyl ether. ^{1}H NMR ($CDCl_3$) δ: 2.56 (s, 3H), 3.68 (t, $J = 4.8$ Hz 2H), 3.75−3.79 (m, 2H) 3.90 (t, $J = 5.1$ Hz, 2H), 4.21 (t, $J = 4.8$ Hz, 2H), 6.96 (d, $J = 8.7$ Hz, 2H), 7.94 (d, $J = 8.7$ Hz, 2H).

1-(4-(2-(2-(2-Hydroxyethoxy)ethoxy)ethoxy)phenyl)ethanone (8c). The reaction described above to prepare **6a** was used, and **8c** was obtained from 4-hydroxyacetophenone and 2-[2-(chloroethoxy)ethoxy]ethanol. ^{1}H NMR ($CDCl_3$) δ: 2.50 (s, 3H), 3.72−3.83 (m, 6H), 3.92 (t, $J = 4.5$ Hz, 2H), 4.22 (t, $J = 5.1$ Hz, 2H), 4.49 (t, $J = 4.2$ Hz, 1H), 4.61 (t, $J = 4.2$ Hz, 1H), 6.86 (d, $J = 8.7$ Hz, 2H), 7.80 (d, $J = 8.7$ Hz, 2H).

1-(4-(2-Fluoroethoxy)phenyl)ethanone (9a). The reaction described above to prepare **7a** was used, and 1.02 g of **9a** was obtained

in a yield of 63.3% from **8a** and DAST. ^{1}H NMR ($CDCl_3$) δ: 4.24 (d, t, J_1 = 28.2 Hz, J_2 = 4.2 Hz, 2H), 4.75 (d, t, J_1 = 47.1 Hz, J_2 = 3.9 Hz, 2H), 6.92 (d, J = 9.0 Hz, 2H), 7.89 (d, J = 9.3 Hz, 2H).

1-(4-(2-(2-Fluoroethoxy)ethoxy)phenyl)ethanone (9b). The reaction described above to prepare **7b** was used, and **9b** was obtained from **9a** and DAST. ^{1}H NMR ($CDCl_3$) δ: 2.56 (s, 3H), 3.78 (t, J = 3.3 Hz, 1H), 3.86–3.94 (m, 3H), 4.22 (t, J = 5.1 Hz, 2H), 4.51 (t, J = 3.0 Hz, 1H), 4.67 (t, J = 3.0.Hz, 1H), 6.96 (d, J = 8.7 Hz, 2H), 7.93 (d, J = 8.7 Hz, 2H). EI-MS: m/z 226 (M^+).

1-(4-(2-(2-(2-Fluoroethoxy)ethoxy)ethoxy)phenyl)ethanone (9c). The reaction described above to prepare **7c** was used, and 543 mg of **9c** was obtained from **8c** and DAST. ^{1}H NMR ($CDCl_3$) δ: 2.56 (s, 3H), 3.69–3.81 (m, 6H), 3.90 (t, J = 4.5 Hz, 2H), 4.21 (t, J = 5.1 Hz, 2H), 4.49 (t, J = 4.2 Hz, 1H), 4.65 (t, J = 4.2 Hz, 1H), 6.95 (d, J = 9.3 Hz, 2H), 7.92 (d, J = 9.0 Hz, 2H). EI-MS: m/z 270 (M^+).

(*E*)-1-(4-(2-Fluoroethoxy)phenyl)-3-(4-nitrophenyl)-2-propen-1-one (10a). The reaction described above to prepare **5** was used, and 856 mg of **10a** was obtained in a yield of 56.6% from **9a** and 4-nitrobenzaldehyde. ^{1}H NMR ($CDCl_3$) δ: 4.32 (d, t, J_1 = 27.6 Hz, J_2 = 4.2 Hz, 2H), 4.81 (d, t, J_1 = 47.4 Hz, J_2 = 4.2 Hz, 2H), 7.04 (d, J = 8.7 Hz, 2H), 7.65 (d, J = 15.6 Hz, 1H), 7.79 (d, J = 8.7 Hz, 2H), 7.82 (d, J = 12.6 Hz, 1H), 8.06 (d, J = 9.0 Hz, 2H), 8.28 (d, J = 8.7 Hz, 2H).

(*E*)-1-(4-(2-(Fluoroethoxy)ethoxy)phenyl)-3-(4-nitrophenyl)-2-propen-1-one (10b). The reaction described above to prepare **5** was used, and 128 mg of **10b** was obtained from **9b** and 4-nitrobenzaldehyde. ^{1}H NMR ($CDCl_3$) δ: 3.79 (t, J = 4.2 Hz, 1H), 3.88–4.27 (m, 3H), 4.8 (t, J = 4.8 Hz, 2H), 4.53 (t, J = 4.2 Hz, 1H), 4.69 (t, J = 4.2 Hz, 1H), 7.03 (d, J = 8.7 Hz, 2H), 7.66 (d, J = 15.6 Hz, 1H), 7.79 (d, J = 9.0 Hz, 2H), 7.81 (d, J = 15.6 Hz, 1H), 8.05 (d, J = 8.7 Hz, 2H), 8.28 (d, J = 9.0 Hz, 2H).

(*E*)-1-(4-(2-((Fluoroethoxy)ethoxy)ethoxy)phenyl)-3-(4-nitrophenyl)-2-propen-1-one (10c). The reaction described above to prepare **5** was used, and 649 mg of **10c** was obtained from **9c**. ^{1}H NMR ($CDCl_3$) δ: 3.71–3.82 (m, 6H), 3.92 (t, J = 4.5 Hz, 2H), 4.24 (t, J = 4.8 Hz, 2H), 4.50 (t, J = 4.2 Hz, 1H), 4.66 (t, J = 4.5 Hz, 1H), 7.03 (d, J = 9.3 Hz, 2H), 7.66 (d, J = 15.6 Hz, 1H), 7.79 (d, J = 9.0 Hz, 2H), 7.81 (d, J = 15.6 Hz, 1H), 8.05 (d, J = 9.3 Hz, 2H), 8.28 (d, J = 8.7 Hz, 2H).

(*E*)-3-(4-Aminophenyl)-1-(4-(2-fluoroethoxy)phenyl)-2-propen-1-one (11a). A mixture of **10a** (856 mg, 2.7 mmol), $SnCl_2$ (2.55 g, 13.5 mmol), and EtOH (10 mL) was stirred at 100 °C for 2 h. After the mixture had cooled to room temperature, 1 M NaOH (10 mL) was added. The mixture was then extracted with ethyl acetate (10 mL). The organic phase was dried over Na_2SO_4 and filtered. The solvent was removed, and the residue was purified by silica gel chromatography using chloroform as a mobile phase to give 333 mg of **11a** (43.0%). ^{1}H NMR ($CDCl_3$) δ: 4.02 (s, broad, 2H), 4.30 (d, t, J_1 = 27.6 Hz, J_2 = 4.2 Hz, 2H), 4.79 (d, t, J_1 = 47.4 Hz, J_2 = 4.2 Hz, 2H), 6.68 (d, J = 8.7 Hz, 2H), 7.00 (d, J = 8.7 Hz, 2H), 7.36 (d, J = 15.3 Hz, 1H), 7.48 (d, J = 8.4 Hz, 2H), 7.75 (d, J = 15.3 Hz, 1H), 8.03 (d, J = 6.9 Hz, 2H). EI-MS: m/z 285 (M^+).

(*E*)-3-(4-Aminophenyl)-1-(4-(2-(fluoroethoxy)ethoxy)phenyl)-2-propen-1-one (11b). The reaction described above to prepare **11a** was used, and 85 mg of **11b** was obtained from **10b**. ^{1}H NMR ($CDCl_3$) δ: 3.77–3.94 (m, 4H), 4.00 (s, broad, 2H), 4.23 (t, J = 4.5 Hz, 2H), 4.53 (t, J = 4.2 Hz, 1H), 4.69 (t, J = 4.2 Hz, 1H), 6.68 (d, J = 8.4 Hz, 2H), 6.99 (d, J = 8.7 Hz, 2H), 7.74 (d, J = 15.6 Hz, 1H), 7.48 (d, J = 8.4 Hz, 1H), 7.36 (d, J = 15.3 Hz, 1H), 8.01 (d, J = 9.0 Hz, 2H). EI-MS: m/z 329 (M^+).

(*E*)-3-(4-Aminophenyl)-1-(4-(2-((fluoroethoxy)ethoxy)ethoxy)-phenyl)-2-propen-1-one (11c). The reaction described above to prepare **11a** was used, and 206 mg of **11c** was obtained from **10c**. ^{1}H NMR ($CDCl_3$) δ: 3.70–3.83 (m, 6H), 3.89 (t, J = 4.5 Hz, 2H), 4.12 (s, broad, 2H), 4.21 (t, J = 4.8 Hz, 2H), 4.49 (t, J = 4.0 Hz, 1H), 4.65 (t, J = 3.9 Hz, 1H), 6.67 (d, J = 8.7 Hz, 2H), 6.98 (d, J = 8.7 Hz, 2H), 7.36 (d, J = 15.3 Hz, 1H), 7.47 (d, J = 8.4 Hz, 2H), 7.74 (d, J = 15.9 Hz, 1H), 8.01 (d, J = 9.0 Hz, 2H). EI-MS: m/z 373 (M^+).

(*E*)-1-(4-(2-Fluoroethoxy)phenyl)-3-(4-(methylamino)phenyl)-2-propen-1-one (12a). To a solution of **11a** (290 mg, 1.02 mmol) in DMSO (6 mL) were added CH_3I (0.18 mL, 3.05 mmol) and anhydrous K_2CO_3 (691 mg, 5.08 mmol). The reaction mixture was stirred at room temperature for 3 h and poured into water. The mixture was extracted with ethyl acetate. The organic layers were combined and dried over Na_2SO_4. Evaporation of the solvent afforded a residue, which was purified by silica gel chromatography (hexane:ethyl acetate = 2:1) to give 90 mg of **12a** (29.5%). ^{1}H NMR ($CDCl_3$) δ: 2.89 (s, 3H), 4.23 (d, t, J_1 = 27.9 Hz, J_2 = 4.2 Hz, 2H), 4.79 (d, t, J_1 = 47.4 Hz, J_2 = 4.2 Hz, 2H), 6.59 (d, J = 8.7 Hz, 2H), 6.99 (d, J = 9.0 Hz, 2H), 7.34 (d, J = 15.3 Hz, 1H), 7.51 (d, J = 8.4 Hz, 2H), 7.78 (d, J = 15.3 Hz, 1H), 8.02 (d, J = 9.3 Hz, 2H). EI-MS: m/z 299 (M^+).

(*E*)-1-(4-(2-(Fluoroethoxy)ethoxy)phenyl)-3-(4-(methylamino)-phenyl)-2-propen-1-one (12b). The reaction described above to prepare **12a** was used, and 22 mg of **12b** was obtained from **11b**. ^{1}H NMR ($CDCl_3$) δ: 2.90 (s, 3H), 3.78–3.95 (m, 4H), 3.99 (s, broad, 1H), 4.23 (t, J = 4.5 Hz, 2H), 4.53 (t, J = 4.5 Hz, 2H), 4.53 (t, J = 4.2 Hz, 1H), 4.69 (t, J = 4.2 Hz, 1H), 6.60 (d, J = 8.7 Hz, 2H), 6.99 (d, J = 8.7 Hz, 2H), 7.35 (d, J = 15.3 Hz, 1H), 7.51 (d, J = 8.7 Hz, 2H), 7.77 (d, J = 15.3 Hz, 1H), 8.02 (d, J = 8.7 Hz, 2H). EI-MS: m/z 343 (M^+).

(*E*)-1-(4-(2-((Fluoroethoxy)ethoxy)ethoxy)phenyl)-3-(4-(methylamino)phenyl)-2-propen-1-one (12c). The reaction described above to prepare **12a** was used, and 53 mg of **12c** was obtained from **11c**. ^{1}H NMR ($CDCl_3$) δ: 2.89 (s, 3H), 3.69–3.83 (m, 6H), 3.90 (t, J = 4.8 Hz, 2H), 4.12 (s, broad, 1H), 4.22 (t, J = 5.1 Hz, 2H), 4.49 (t, J = 4.2 Hz, 1H), 4.65 (t, J = 4.1 Hz, 1H), 6.60 (d, J = 8.7 Hz, 2H), 6.98 (d, J = 9.0 Hz, 2H), 7.35 (d, J = 15.3 Hz, 1H), 7.51 (d, J = 8.7 Hz, 2H), 7.76 (d, J = 15.3 Hz, 1H), 8.01 (d, J = 8.7 Hz, 2H). EI-MS: m/z 387 (M^+).

(*E*)-3-(4-Dimethylaminophenyl)-1-(4-fluorophenyl)-2-propen-1-one (13). The reaction described above to prepare **5** was used, and 209 mg of **13** was obtained from 4-fluoroacetophenone and 4-dimethylbenzaldehyde. ^{1}H NMR (300 MHz, $CDCl_3$) δ: 3.03 (s, 6H), 6.68 (d, J = 8.7 Hz, 2H), 7.15 (t, J = 8.4 Hz, 2H), 7.30 (d, J = 15.3 Hz, 1H), 7.54 (d, J = 9.0 Hz, 2H), 7.78 (d, J = 15.3 Hz, 1H), 8.02–8.06 (m, 2H). EI-MS: m/z 269 (M^+).

(*E*)-1-(4-Fluorophenyl)-3-(4-nitrophenyl)-2-propen-1-one (14). The reaction described above to prepare **5** was used, and 490 mg of **14** was obtained from 4-fluoroacetophenone and 4-nitrobenzaldehyde. ^{1}H NMR (300 MHz, $CDCl_3$) δ: 7.21 (t, J = 8.7 Hz, 2H), 7.62 (d, J = 15.9 Hz, 1H), 7.80 (d, J = 8.7 Hz, 2H), 7.84 (d, J = 15.9 Hz, 1H), 8.07–8.12 (m, 2H), 8.29 (d, J = 8.7 Hz, 2H). EI-MS: m/z 271 (M^+).

(*E*)-3-(4-Aminophenyl)-1-(4-fluorophenyl)-2-propen-1-one (15). The reaction described above to prepare **11(a–c)** was used, and 150 mg of **15** was obtained from **14**. ^{1}H NMR (300 MHz, $CDCl_3$) δ: 4.07 (s, broad, 2H), 6.67 (d, J = 8.7 Hz, 2H), 7.15 (t, J = 8.7 Hz, 2H), 7.31 (d, J = 15.6 Hz, 1H), 7.47 (d, J = 8.4 Hz, 2H), 7.75 (d, J = 15.6 Hz, 1H), 8.03 (t, J = 8.7 Hz, 2H). EI-MS: m/z 241 (M^+).

(*E*)-1-(4-Fluorophenyl)-3-(4-methylaminophenyl)-2-propen-1-one (16). The reaction described above to prepare **12(a–c)** was used, and 14 mg of **16** was obtained from **15**. ^{1}H NMR (300 MHz, $CDCl_3$) δ: 2.90 (s, 3H), 4.20 (s, broad, 1H), 6.60 (d, J = 8.7 Hz, 2H), 7.17 (d, J = 8.7 Hz, 2H), 7.30 (d, J = 15.6 Hz, 1H), 7.50 (d, J = 8.7 Hz, 2H), 7.78 (d, J = 15.6 Hz, 1H), 8.04 (d, J = 8.7 Hz, 2H). EI-MS: m/z 255 (M^+).

(*E*)-2-(2-(2-(4-(3-(4-(Dimethylamino)phenyl)acryloyl)phenoxy)-ethoxy)ethoxy)ethyl 4-methylbenzenesulfonate (17). To a solution of **6c** (108 mg, 0.27 mmol) in pyridine (3 mL) was added tosyl chloride (343.8 mg, 0.621 mmol). The reaction mixture was stirred for 3 h at room temperature. After water was added, the mixture was extracted with ethyl acetate. The organic layer was dried over Na_2SO_4, and evaporation of the solvent afforded a residue, which was purified by preparative TLC (hexane:ethyl acetate = 1:1) to give 44 mg of **17** (29.4%). ^{1}H NMR (300 MHz, $CDCl_3$) δ: 2.43 (s, 3H), 3.04 (s, 6H), 3.62–3.72 (m, 6H),

3.85−3.87 (m, 2H), 4.15−4.18 (m, 4H), 6.70 (d, J = 8.7 Hz, 2H), 6.98 (d, J = 9.0 Hz, 2H), 7.31−7.35 (m, 2H), 7.37 (d, J = 9.0 Hz, 1H), 7.55 (d, J = 8.7 Hz, 2H), 7.80 (t, J = 8.7 Hz, 3H), 8.02 (d, J = 9.0 Hz, 2H). EI-MS m/z 553 (M^+)

Radiolabeling. Procedure for Labeling of 7a, 7b, 7c, and 13 with ^{11}C. ^{11}C was produced via a ^{14}N(p,α)^{11}C reaction with 16 MeV protons on a target of nitrogen gas with an ultracompact cyclotron (CYPRIS model 325R; Sumitomo Heavy Industry Ltd.) The $^{11}CO_2$ produced was transported to an automated system for the synthesis of ^{11}C-methyl iodide (CUPID C-100; Sumitomo Heavy Industry Ltd.) and converted sequentially to [^{11}C]MeOTf by the previously described method of Jewett.[33] [^{11}C]Chalcones were produced by reacting [^{11}C]MeOTf with the normethyl precursor, **7a**, **7b**, **7c**, and **13**, (0.5 mg) in 500 μL of methyl ethyl ketone (MEK). After the complete transfer of [^{11}C]MeOTf, ^{11}C-methylation was carried out for 5 min and the reaction solvent was then dried with a stream of nitrogen gas. The residue taken up in 200 μL of acetonitrile was purified by a reverse phase HPLC system (a Shimadzu LC-6A isocratic pump, a Shimadzu SPD-6A UV detector, and a Aloka NDW-351D scintillation detector) on a Cosmosil $5C_{18}$ column (Nakalai Tesque, $5C_{18}$-AR-II, 10 mm × 250 mm) with an isocratic solvent of acetonitrile/water (55/45) at a flow rate of 6.0 mL/min. The desired fraction was collected in a flask and evaporated dry. The radiochemical yield, purity, and specific activity of [^{11}C]chalcones were further confirmed by analytical reverse phase HPLC on a $5C_{18}$-AR-300 column (Nakalai Tesque, 4.6 mm × 150 mm, acetonitrile/water (60/40), 1.0 mL/min).

Procedure for Labeling 7c with ^{18}F. [^{18}F]Fluoride was produced by the JSW typeBC3015 cyclotron via an ^{18}O(p,n)^{18}F reaction and passed through a Sep-Pak Light QMA cartridge (Waters) as an aqueous solution in ^{18}O-enriched water. The cartridge was dried by airflow, and the ^{18}F activity was eluted with 0.5 mL of a Kryptofix 222/K_2CO_3 solution (11 mg of Kryptofix 222 and 2.6 mg of K_2CO_3 in acetonitrile/water (86/14)). The solvent was removed at 120 °C under a stream of argon gas. The residue was azeotropically dried with 1 mL of anhydrous acetonitrile twice at 120 °C under a stream of nitrogen gas and dissolved in DMSO (1 mL). A solution of tosylate precursor **17** (1.0 mg) in DMSO (1 mL) was added to the reaction vessel containing the ^{18}F activity in DMSO. The mixture was heated at 160 °C for 5 min. Water (5 mL) was added, and the mixture was passed through a preconditioned Oasis HLB cartridge (3 cm^3) (Waters). The cartridge was washed with 10 mL of water, and the labeled compound was eluted with 2 mL of acetonitrile. The eluted compound was purified by preparative HPLC [YMC-Pack Pro C_{18} column (20 mm × 150 mm), acetonitrile/water (75/25), flow rate 9.0 mL/min]. The retention time of the major byproduct of hydrolysis (t_R = 2.7 min) was well-resolved from the desired ^{18}F-labeled product (t_R = 10.7 min). The radiochemical purity and specific activity were determined by analytical HPLC [YMC-Pack Pro C_{18} column (4.6 mm × 150 mm), acetonitrile/water (60/40), flow rate 1.0 mL/min], and [^{18}F]**7c** was obtained in a radiochemical purity of >99% with the specific activity of 35 GBq/mmol. Specific activity was estimated by comparing the UV peak intensity of the purified ^{18}F-labeled compound with a reference nonradioactive compound of known concentration.

Binding Assays Using the Aggregated Aβ peptides in Solution. Aβ(1−42) was purchased from Peptide Institute (Osaka, Japan). Aggregation was carried out by gently dissolving the peptide (0.25 mg/mL) in a buffer solution (pH 7.4) containing 10 mM sodium phosphate and 1 mM EDTA. The solution was incubated at 37 °C for 42 h with gentle and constant shaking. Binding experiments were carried out as described previously.[18] [^{125}I]DMIC with 2200 Ci/mmol of specific activity and radiochemical purity greater than 95% was prepared using the standard iododestannylation reaction. A mixture containing 50 μL of test compound (0.2 pM-400 μM in 10% EtOH), 50 μL of 0.02 nM [^{125}I]DMIC, 50 μL of Aβ(1−42) aggregates, and 850 μL of 10% EtOH was incubated at room temperature for 3 h. The mixture was then filtered through Whatman GF/B filters using a Brandel M-24 cell harvester, and the radioactivity of the filters containing the bound ^{125}I ligand was measured in a γ counter. Values for the half-maximal inhibitory concentration (IC_{50}) were determined from displacement curves of three independent experiments using GraphPad Prism 4.0, and those for the inhibition constant (K_i) were calculated using the Cheng−Prusoff equation: $K_i = IC_{50}/(1 + [L]/K_d)$, where [L] is the concentration of [^{125}I]DMIC used in the assay and K_d is the dissociation constant of DMIC (4.2 nM).[19] DMIC and IMPY used as test compounds for the inhibition assay were synthesized as reported previously.[19,34]

Biodistribution in Normal Mice. Experiments with animals were conducted in accordance with our institutional guidelines and approved by the Nagasaki University Animal Care Committee and the Kyoto University Animal Care Committee. A 100 μL amount of a saline solution containing the radiolabeled agent (3.7 MBq), EtOH (10%), and ascorbic acid (1 mg/mL) was injected directly into the tail vein of ddY mice (5-week-old, 22−25 g). Groups of five mice were sacrificed at various post-injection time points. The organs of interest were removed and weighed, and the radioactivity was measured with an automatic γ counter (COBRAII, Packard).

Staining of Aβ Plaques in Brain Sections of Tg2576 Transgenic Mice. The Tg2576 transgenic mice (female, 20-month-old) and wild-type (female, 20-month-old) mice were used as an Alzheimer's model and an age-matched control, respectively. After the mice were sacrificed by decapitation, the brains were immediately removed and frozen in powdered dry ice. The frozen blocks were sliced into serial sections 10 μm thick. Each slide was incubated with a 50% EtOH solution (100 μM) of compound **7c** for 10 min. The sections were washed with 50% EtOH for 3 min two times. After drying, the sections were then examined using a microscope (Nikon, Eclipse 80i) equipped with a B-2A filter set (excitation, 450−490 nm; diachronic mirror, 505 nm; long-pass filter, 520 nm). Thereafter, the serial sections were also immunostained with 3,3′-diaminobenzidine (DAB) as a chromogen using monoclonal antibodies against Aβ (amyloid β-protein immunohistostain kit, WAKO).

In Vitro Autoradiography Using Human AD Brains. Postmortem brain tissues from an autopsy-confirmed case of AD (73-year-old male) were obtained from BioChain Institute Inc. The presence and localization of plaques on the sections were confirmed with immunohistochemical staining using a monoclonal Aβ antibody as described above. The sections were incubated with [^{18}F]**7c** (54 μCi/200 μL) for 1 h at room temperature. They were then washed in 50% EtOH (two 1 min wash), before being rinsed with water for 30 s. After drying, the ^{18}F-labeled sections were exposed to a BAS imaging plate (Fuji Film, Tokyo, Japan) for 6 h. Ex vivo autoradiographic images were obtained using a BAS5000 scanner system (Fuji Film). After autoradiographic examination, the same sections were stained by thioflavin-S to confirm the presence of Aβ plaques. For the staining of thioflavin-S, sections were immersed in a 0.125% thioflavin-S solution containing 50% EtOH for 3 min and washed in 50% EtOH. After drying, the sections were then examined using a microscope (Nikon, Eclipse 80i) equipped with a B-2A filter set (excitation, 450−490 nm; diachronic mirror, 505 nm; long-pass filter, 520 nm).

Acknowledgment. This study was supported by the Program for Promotion of Fundamental Studies in Health Sciences of the National Institute of Biomedical Innovation (NIBIO), a Health Labour Sciences Research Grant, and a Grant-in-Aid for Young Scientists (A) and Exploratory Research from the Ministry of Education, Culture, Sports, Science and Technology, Japan.

Supporting Information Available: Representative HPLC chromatograms of [^{18}F]**7c**. This material is available free of charge via the Internet at http://pubs.acs.org.

References

(1) Hardy, J. A.; Higgins, G. A. Alzheimer's disease: the amyloid cascade hypothesis. *Science* **1992**, *256*, 184–185.

(2) Selkoe, D. J. Alzheimer's disease: genes, proteins, and therapy. *Physiol. Rev.* **2001**, *81*, 741–766.

(3) Nordberg, A. PET imaging of amyloid in Alzheimer's disease. *Lancet Neurol.* **2004**, *3*, 519–527.

(4) Mathis, C. A.; Wang, Y.; Klunk, W. E. Imaging β-amyloid plaques and neurofibrillary tangles in the aging human brain. *Curr. Pharm. Des.* **2004**, *10*, 1469–1492.

(5) Klunk, W. E.; Engler, H.; Nordberg, A.; Wang, Y.; Blomqvist, G.; Holt, D. P.; Bergstrom, M.; Savitcheva, I.; Huang, G. F.; Estrada, S.; Ausen, B.; Debnath, M. L.; Barletta, J.; Price, J. C.; Sandell, J.; Lopresti, B. J.; Wall, A.; Koivisto, P.; Antoni, G.; Mathis, C. A.; Langstrom, B. Imaging brain amyloid in Alzheimer's disease with Pittsburgh Compound-B. *Ann. Neurol.* **2004**, *55*, 306–319.

(6) Mathis, C. A.; Wang, Y.; Holt, D. P.; Huang, G. F.; Debnath, M. L.; Klunk, W. E. Synthesis and evaluation of ^{11}C-labeled 6-substituted 2-arylbenzothiazoles as amyloid imaging agents. *J. Med. Chem.* **2003**, *46*, 2740–2754.

(7) Verhoeff, N. P.; Wilson, A. A.; Takeshita, S.; Trop, L.; Hussey, D.; Singh, K.; Kung, H. F.; Kung, M. P.; Houle, S. In vivo imaging of Alzheimer disease β-amyloid with [^{11}C]SB-13 PET. *Am. J. Geriatr. Psychiatry* **2004**, *12*, 584–595.

(8) Ono, M.; Wilson, A.; Nobrega, J.; Westaway, D.; Verhoeff, P.; Zhuang, Z. P.; Kung, M. P.; Kung, H. F. ^{11}C-Labeled stilbene derivatives as Abeta-aggregate-specific PET imaging agents for Alzheimer's disease. *Nucl. Med. Biol.* **2003**, *30*, 565–571.

(9) Small, G. W.; Kepe, V.; Ercoli, L. M.; Siddarth, P.; Bookheimer, S. Y.; Miller, K. J.; Lavretsky, H.; Burggren, A. C.; Cole, G. M.; Vinters, H. V.; Thompson, P. M.; Huang, S. C.; Satyamurthy, N.; Phelps, M. E.; Barrio, J. R. PET of brain amyloid and tau in mild cognitive impairment. *N. Engl. J. Med.* **2006**, *355*, 2652–2663.

(10) Shoghi-Jadid, K.; Small, G. W.; Agdeppa, E. D.; Kepe, V.; Ercoli, L. M.; Siddarth, P.; Read, S.; Satyamurthy, N.; Petric, A.; Huang, S. C.; Barrio, J. R. Localization of neurofibrillary tangles and β-amyloid plaques in the brains of living patients with Alzheimer disease. *Am. J. Geriatr. Psychiatry* **2002**, *10*, 24–35.

(11) Rowe, C. C.; Ackerman, U.; Browne, W.; Mulligan, R.; Pike, K. L.; O'Keefe, G.; Tochon-Danguy, H.; Chan, G.; Berlangieri, S. U.; Jones, G.; Dickinson-Rowe, K. L.; Kung, H. P.; Zhang, W.; Kung, M. P.; Skovronsky, D.; Dyrks, T.; Holl, G.; Krause, S.; Friebe, M.; Lehman, L.; Lindemann, S.; Dinkelborg, L. M.; Masters, C. L.; Villemagne, V. L. Imaging of amyloid β in Alzheimer's disease with ^{18}F-BAY94-9172, a novel PET tracer: proof of mechanism. *Lancet Neurol.* **2008**, *7*, 129–135.

(12) Zhang, W.; Oya, S.; Kung, M. P.; Hou, C.; Maier, D. L.; Kung, H. F. F-18 polyethyleneglycol stilbenes as PET imaging agents targeting Aβ aggregates in the brain. *Nucl. Med. Biol.* **2005**, *32*, 799–809.

(13) Lockhart, A. Imaging Alzheimer's disease pathology: one target, many ligands. *Drug Discovery Today* **2006**, *11*, 1093–1099.

(14) Ye, L.; Morgenstern, J. L.; Gee, A. D.; Hong, G.; Brown, J.; Lockhart, A. Delineation of positron emission tomography imaging agent binding sites on β-amyloid peptide fibrils. *J. Biol. Chem.* **2005**, *280*, 23599–235604.

(15) Lockhart, A.; Ye, L.; Judd, D. B.; Merritt, A. T.; Lowe, P. N.; Morgenstern, J. L.; Hong, G.; Gee, A. D.; Brown, J. Evidence for the presence of three distinct binding sites for the thioflavin T class of Alzheimer's disease PET imaging agents on β-amyloid peptide fibrils. *J. Biol. Chem.* **2005**, *280*, 7677–7684.

(16) Ono, M.; Yoshida, N.; Ishibashi, K.; Haratake, M.; Arano, Y.; Mori, H.; Nakayama, M. Radioiodinated flavones for in vivo imaging of β-amyloid plaques in the brain. *J. Med. Chem.* **2005**, *48*, 7253–7260.

(17) Ono, M.; Watanabe, R.; Kawashima, H.; Kawai, T.; Watanabe, H.; Haratake, M.; Saji, H.; Nakayama, M. ^{18}F-Labeled flavones for in vivo imaging of β-amyloid plaques in Alzheimer's brains. *Bioorg. Med. Chem.* **2009**, *17*, 2069–2076.

(18) Ono, M.; Hori, M.; Haratake, M.; Tomiyama, T.; Mori, H.; Nakayama, M. Structure–activity relationship of chalcones and related derivatives as ligands for detecting of β-amyloid plaques in the brain. *Bioorg. Med. Chem.* **2007**, *15*, 6388–6396.

(19) Ono, M.; Haratake, M.; Mori, H.; Nakayama, M. Novel chalcones as probes for in vivo imaging of β-amyloid plaques in Alzheimer's brains. *Bioorg. Med. Chem.* **2007**, *15*, 6802–6809.

(20) Maya, Y.; Ono, M.; Watanabe, H.; Haratake, M.; Saji, H.; Nakayama, M. Novel radioiodinated aurones as probes for SPECT imaging of β-amyloid plaques in the brain. *Bioconjugate Chem.* **2009**, *20*, 95–101.

(21) Ono, M.; Maya, Y.; Haratake, M.; Ito, K.; Mori, H.; Nakayama, M. Aurones serve as probes of β-amyloid plaques in Alzheimer's disease. *Biochem. Biophys. Res. Commun.* **2007**, *361*, 116–121.

(22) Stephenson, K. A.; Chandra, R.; Zhuang, Z. P.; Hou, C.; Oya, S.; Kung, M. P.; Kung, H. F. Fluoro-pegylated (FPEG) imaging agents targeting Aβ aggregates. *Bioconjugate Chem.* **2007**, *18*, 238–246.

(23) Qu, W.; Kung, M. P.; Hou, C.; Oya, S.; Kung, H. F. Quick assembly of 1,4-diphenyltriazoles as probes targeting β-amyloid aggregates in Alzheimer's disease. *J. Med. Chem.* **2007**, *50*, 3380–3387.

(24) Zhang, W.; Oya, S.; Kung, M. P.; Hou, C.; Maier, D. L.; Kung, H. F. F-18 stilbenes as PET imaging agents for detecting β-amyloid plaques in the brain. *J. Med. Chem.* **2005**, *48*, 5980–5988.

(25) Kung, M. P.; Hou, C.; Zhuang, Z. P.; Zhang, B.; Skovronsky, D.; Trojanowski, J. Q.; Lee, V. M.; Kung, H. F. IMPY: an improved thioflavin-T derivative for in vivo labeling of β-amyloid plaques. *Brain Res.* **2002**, *956*, 202–210.

(26) Hsiao, K.; Chapman, P.; Nilsen, S.; Eckman, C.; Harigaya, Y.; Younkin, S.; Yang, F.; Cole, G. Correlative memory deficits, Aβ elevation, and amyloid plaques in transgenic mice. *Science* **1996**, *274*, 99–102.

(27) Kuntner, C.; Kesner, A. L.; Bauer, M.; Kremslehner, R.; Wanek, T.; Mandler, M.; Karch, R.; Stanek, J.; Wolf, T.; Muller, M.; Langer, O. Limitations of small animal PET imaging with [^{18}F]FDDNP and FDG for quantitative studies in a transgenic mouse model of Alzheimer's disease. *Mol. Imaging Biol.* **2009**, *11*, 236–240.

(28) Klunk, W. E.; Lopresti, B. J.; Ikonomovic, M. D.; Lefterov, I. M.; Koldamova, R. P.; Abrahamson, E. E.; Debnath, M. L.; Holt, D. P.; Huang, G. F.; Shao, L.; DeKosky, S. T.; Price, J. C.; Mathis, C. A. Binding of the positron emission tomography tracer Pittsburgh compound-B reflects the amount of amyloid-β in Alzheimer's disease brain but not in transgenic mouse brain. *J. Neurosci.* **2005**, *25*, 10598–10606.

(29) Maeda, J.; Ji, B.; Irie, T.; Tomiyama, T.; Maruyama, M.; Okauchi, T.; Staufenbiel, M.; Iwata, N.; Ono, M.; Saido, T. C.; Suzuki, K.; Mori, H.; Higuchi, M.; Suhara, T. Longitudinal, quantitative assessment of amyloid, neuroinflammation, and anti-amyloid treatment in a living mouse model of Alzheimer's disease enabled by positron emission tomography. *J. Neurosci.* **2007**, *27*, 10957–10968.

(30) Toyama, H.; Ye, D.; Ichise, M.; Liow, J. S.; Cai, L.; Jacobowitz, D.; Musachio, J. L.; Hong, J.; Crescenzo, M.; Tipre, D.; Lu, J. Q.; Zoghbi, S.; Vines, D. C.; Seidel, J.; Katada, K.; Green, M. V.; Pike, V. W.; Cohen, R. M.; Innis, R. B. PET imaging of brain with the β-amyloid probe, [^{11}C]6-OH-BTA-1, in a transgenic mouse model of Alzheimer's disease. *Eur. J. Nucl. Med. Mol. Imaging* **2005**, *32*, 593–600.

(31) Skovronsky, D. M.; Zhang, B.; Kung, M. P.; Kung, H. F.; Trojanowski, J. Q.; Lee, V. M. In vivo detection of amyloid plaques in a mouse model of Alzheimer's disease. *Proc. Natl. Acad. Sci. U.S.A* **2000**, *97*, 7609–7614.

(32) Saido, T. C.; Iwatsubo, T.; Mann, D. M.; Shimada, H.; Ihara, Y.; Kawashima, S. Dominant and differential deposition of distinct β-amyloid peptide species, A β N3(pE), in senile plaques. *Neuron* **1995**, *14*, 457–466.

(33) Jewett, D. M. A simple synthesis of [^{11}C]methyl triflate. *Int. J. Radiat. Appl. Instrum. A* **1992**, *43*, 1383–1385.

(34) Zhuang, Z. P.; Kung, M. P.; Wilson, A.; Lee, C. W.; Plossl, K.; Hou, C.; Holtzman, D. M.; Kung, H. F. Structure–activity relationship of imidazo[1,2-*a*]pyridines as ligands for detecting β-amyloid plaques in the brain. *J. Med. Chem.* **2003**, *46*, 237–243.

—Reviews—

PET/SPECTによる分子イメージング研究

小野正博

Molecular Imaging by PET/SPECT

Masahiro ONO

Department of Patho-Functional Bioanalysis, Graduate School of Pharmaceutical Sciences, Kyoto University, 46–29 Yoshida Shimoadachi-cho, Sakyo-ku, Kyoto 606–8501, Japan

(Received September 19, 2008)

Molecular imaging by PET/SPECT with radiopharmaceuticals enables noninvasively quantitative evaluation of physiological function, gene expression, pharmacokinetics of proteins and peptides and distribution of receptors with high sensitivity. Together with recent development of imaging equipments, molecular imaging by PET/SPECT is expected to contribute to elucidation of physiological and pathological functions, medical sciences and clinical diagnoses. Molecular imaging with radiopharmaceuticals started from diagnosis of cancer with ^{18}F-2-fluoro-2-deoxyglucose ([^{18}F]FDG). Currently, [^{18}F]FDG is commonly used in the field of clinical diagnosis, because it can provide qualitative information on malignancy and metastasis of tumor. Since its achievement, much effort has been devoted to the development of radiopharmaceuticals that bind or interact with the *in vivo* biomarkers. For example, a number of radiopharmaceuticals based on proteins and peptides with high binding affinities to various biomarkers have been applied for the diagnosis of tumor, arteriosclerosis, thrombus and so on. Furthermore, Alzheimer's disease is also a major target for diagnosis by PET/SPECT imaging. The development of low-molecular-weight radiolabeled probes for the quantitation of β-amyloid plaques and neurofibrillary tangles in Alzheimer's brains is a topic of current PET/SPECT imaging studies. Here, some recent progress and development of radiopharmaceuticals for PET/SPECT imaging will be reviewed.

Key words——molecular imaging; radiopharmaceutical; tumor; positron emission tomography (PET); single photon emission computed tomography (SPECT); β-amyloid

1. はじめに

体内における遺伝子やタンパク質などの分子を生物が生きたままの状態で画像化する「分子イメージング」は，様々な病態に関与する分子を画像化することで疾患の高度な診断を可能にすると考えられている．分子イメージングには，PET (positron emission tomography)/SPECT (single photon emission computed tomography)，光イメージング，磁気共鳴イメージング (MRI) などが汎用されているが，中でもPET/SPECTによる分子イメージングは，放射性核種 (radioisotope, RI) で標識した放射性化合物を生体内に投与し，標的部位に分布あるいは標的分子に結合した放射性化合物から放出されるガンマ線を体外より検出，定量画像化する技術である．このような特徴を生かして，PET/SPECTによる分子イメージングは現在，生体機能の病因の解明，再生医療，テーラーメード医療などの医学研究，創薬研究，臨床診断分野などへの貢献が期待されている．

PET/SPECTのインビボイメージングに用いられるRIは，ポジトロン放出核種 (PET核種) とシングルフォトン放出核種 (SPECT核種) の2種類に大別される．PET核種は，β^+ 崩壊により生成する陽電子が陰電子と結合し，511 keVの2本のガンマ線を180°方向に同時に放出する核種であり，^{11}C, ^{13}N, ^{15}O, ^{18}Fなどが用いられる．SPECT核種は，電子捕獲や核異性体転移により単一のガンマ線を放出する核種であり，インビボイメージングに用いられる核種として，^{67}Ga, ^{99m}Tc, ^{111}In, ^{123}Iなどが挙げられる．これらのPET核種の半減期は，2分から110分と非常に短いのに対して，SPECT核種は，

京都大学大学院薬学研究科病態機能分析学分野 (〒606–8501 京都市左京区吉田下阿達町 46–29)
e-mail: ono@pharm.kyoto-u.ac.jp

本総説は，日本薬学会第128年会シンポジウムS36で発表したものを中心に記述したものである．

数時間から数十時間の半減期であるという点で異なる（Table 1）.

一般的に分子イメージングプローブに求められる条件としては，合成が容易で，収率が高く，生体内に投与後，できるだけ短時間に標的部位へ移行し，高い標的／非標的比が得られること，安全性が高いことなどが挙げられる．また PET/SPECT 用分子プローブでは，さらに短半減期の核種で標識する必要があるため，1）迅速な合成ができること，2）微量でも定量的に反応が進行すること，3）高い放射化学的収率及び放射化学的純度で得られること，4）代謝の影響等を受けない部位に選択的に標識できることなどの条件も必要となる.

2. PET/SPECT による腫瘍の分子イメージング

次に，PET/SPECT を用いた腫瘍の分子イメージングについて紹介する．現在，腫瘍のイメージング剤として最も臨床で利用されているのが，[^{18}F]FDG（2-deoxy-2-[^{18}F]-fluoro-D-glucose）である（Fig. 1）．[^{18}F]FDG は，グルコースの 2 位の水酸基を ^{18}F に置換した構造をしており，グルコースと同様に，グルコーストランスポータにより，血液から細胞内に取り込まれ，ヘキソキナーゼによって 6 位リン酸化を受けるが，生成した [^{18}F]FDG-6 リン酸（2-deoxy-2-fluoro-D-glucose-6-phosphate）は，それ以降の解糖系酵素の基質とならないため細胞内に滞留する．したがって，[^{18}F]FDG の細胞内への集積はグルコーストランスポータとヘキソキナーゼの活性により決まり，グルコーストランスポータの発現とヘキソキナーゼ活性が亢進している腫瘍細胞では [^{18}F]FDG の高い集積を示し，腫瘍のイメージングが可能になる．本邦においても，2002 年 4 月から [^{18}F]FDG-PET が保険適用され，PET 検査数は急激な増加傾向にある．しかしながら，あくまで [^{18}F]FDG は，細胞のグルコース代謝を反映しており，腫瘍に特異的ではないこと，脳への生理的集積が高いこと，炎症部位にも集積することなどの問題を有しており，現在，[^{18}F]FDG より腫瘍特異性の高い分子プローブの開発が活発に行われている．これまでに，[^{18}F]FDG 以外にも，多くの PET/SPECT 用腫瘍分子イメージングプローブが報告されており，2 種類に大別される（Table 2）．1 つは，腫瘍細胞で亢進した生体機能に着目したプローブであり，核酸代謝イメージング剤，[1] アミノ酸代謝イメージング剤，[2] 膜脂質代謝イメージング剤[3] などが開発されている．もう 1 つは，腫瘍部位の組織環境・特異的発現分子に着目したプローブであり，腫瘍の低酸素部位イメージング剤である，ニトロイミダゾール誘導体，[4] 銅キレート錯体，[5] アポトーシスのイメージング剤，[6] 腫瘍細胞に多く発現したソマトスタチンレセプターを標的にした，レセプタ発現イメージング剤，[7] 血管新生の際に高い発現を示す，$\alpha_v\beta_3$ インテグリンレセプターを標的に

Table 1. Radioisotopes Used for PET/SPECT Imaging

核　種	物理的半減期	放射線エネルギー (keV)
ポジトロン放出核種		
^{11}C	20.39 m	511
^{13}N	9.96 m	511
^{15}O	122 s	511
^{18}F	109.8 m	511
シングルフォトン放出核種		
^{67}Ga	78.3 h	93, 185, 300
^{99m}Tc	6.01 h	141
^{111}In	2.81 d	171, 245
^{123}I	13.3 h	159

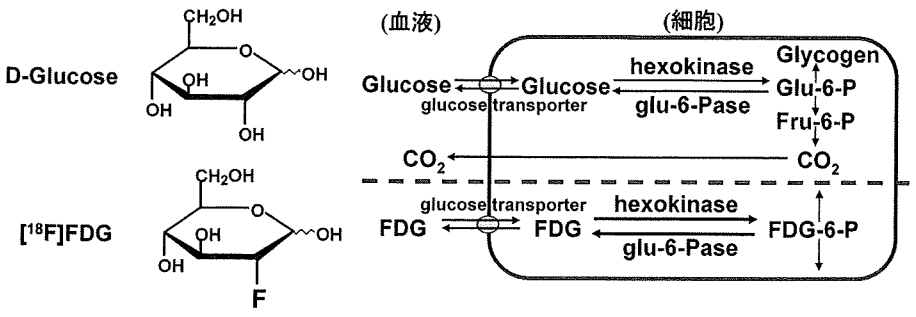

Fig. 1. Mechanism of Cellular Uptake of [^{18}F]FDG

Table 2. Tumor Imaging Probes for PET/SPECT

腫瘍細胞で亢進した生体機能に着目したプローブ	腫瘍部位の組織環境，特異的発現分子に着目したプローブ
糖代謝イメージング	低酸素部位イメージング
グルコース誘導体：[^{18}F] FDG	ニトロイミダゾール誘導体
糖代謝イメージング	[^{18}F] FMISO, [^{18}F] FAZA
核酸誘導体：[^{18}F] FLT	銅キレート化合物
アミノ酸代謝イメージング	[$^{62/64}$Cu] ATSM
アミノ酸，アミノ酸誘導体	アポトーシスイメージング
[^{11}C] メチオニン，[^{18}F] FET, [^{18}F]	[^{18}F/^{99m}Tc] annexin V
FAMT, [^{18}F] FACBC	レセプタ発現イメージング
膜脂質代謝イメージング	[^{18}F/^{111}In/^{99m}Tc] オクトレオタイド
コリン，コリン誘導体	血管新生イメージング
[^{18}F] フルオロコリン，[^{18}F] コリン	[^{18}F/^{111}In/^{99m}Tc] RGD ペプチド
	放射免疫シンチグラフィー
	[^{111}In/^{99m}Tc] 抗体，抗体フラグメント

したイメージング剤,[8] また，がん細胞表面に発現したがん抗原に対する抗体を用いる，放射免疫シンチグラフィ[9]などが知られている．[^{18}F]FDG を含めて，核酸代謝イメージング剤，アミノ酸代謝イメージング剤，膜脂質代謝イメージング剤，低酸素部位のイメージング剤は，いずれも低分子化合物であるのに対して，アポトーシスのイメージング剤，レセプタ発現イメージング剤，血管新生イメージング剤，放射免疫シンチグラフィに用いられるプローブは，タンパク質・ペプチドを基盤とするものであり，そのプローブの設計は大きく異なる．

そこで次に，タンパク質・ペプチドを基盤とした腫瘍の分子イメージングプローブについて紹介する．タンパク質・ペプチドを基盤とする分子プローブは，腫瘍指向性のタンパク質・ペプチドの標的分子の結合部位とは独立して，同一分子内に RI の結合部位を有する二官能性放射性薬剤のことを言い，腫瘍指向性のタンパク質・ペプチドが RI のキャリアとして，腫瘍部位へ放射能を送達する．腫瘍指向性のタンパク質・ペプチドとしては，抗腫瘍抗体，そのフラグメント，オクトレオタイド，RGD ペプチドなどが利用されている．この二官能性放射性薬剤の原理は，腫瘍イメージングに限らず，ほかの病態に対するタンパク質・ペプチドを使用することにより様々な病態の診断にも応用できることから，多くの放射性プローブの開発に応用されている．二官能性放射性薬剤には，SPECT 用 RI である，^{67}Ga, ^{99m}Tc, ^{111}In がよく使われる．しかし一般的に，金属 RI は，タンパク質・ペプチドと直接安定に結合しないため，二官能性放射性薬剤の作製には，同一分子内にタンパク質・ペプチドとの結合部位と金属 RI とのキレート形成部位とを併せ持つ，二官能性キレート試薬が必要である（Fig. 2）．

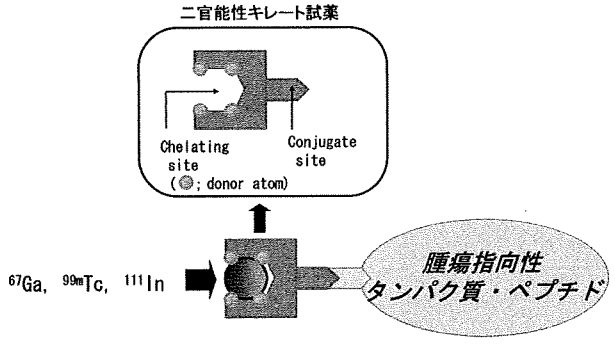

Fig. 2. Bifuctional Chelating Agents to Label Proteins and Peptides with Metal Radioiosotopes

われわれは，腫瘍のイメージングを目的とした抗腫瘍抗体 Fab フラグメントの ^{99m}Tc 標識体を作製するために，6-hydrazinonicotinamide-3-carboxylic acid (HYNIC) を二官能性キレート試薬として選択した．HYNIC は，hydrazinopyridine をキレート部位，カルボン酸を抗体フラグメントのリジン残基との結合とする化合物であり，補助配位子として，トリシンとベンゾイルピリジン（BP）を用いて，抗体 Fab フラグメントを ^{99m}Tc で標識した，^{99m}Tc-(HYNIC-Fab) (tricine) (BP) を作製し，腫瘍移植マウスを用いる検討を行った（Fig. 3）．^{99m}Tc 標識 Fab フラグ

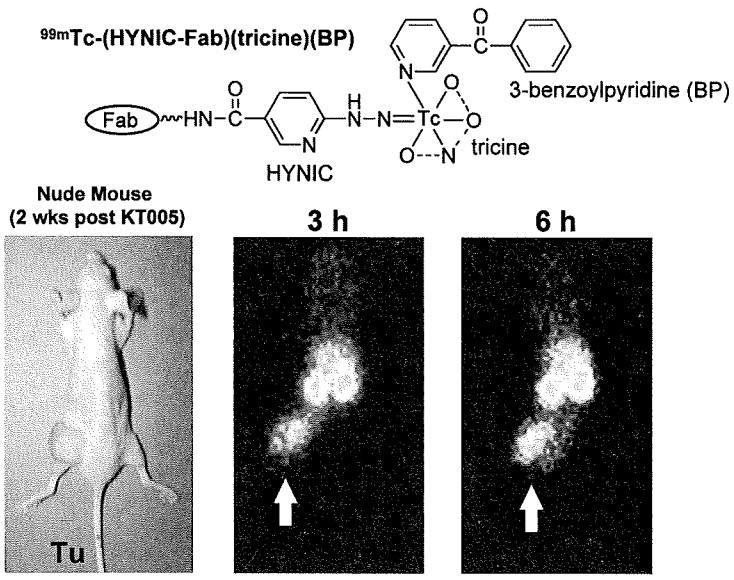

Fig. 3. Tumor Imaging in a Model Mouse with ^{99m}Tc-(HYNIC-Fab) (tricine) (BP)

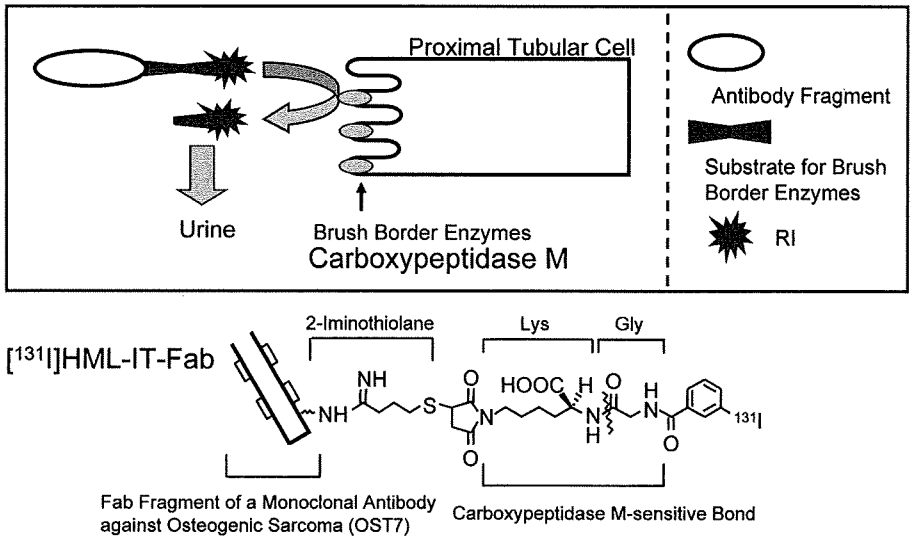

Fig. 4. Brush Border Strategy to Reduce Radioactivity Level in the Kidney

メントを腫瘍移植マウスに投与3及び6時間後の腫瘍と血液の放射能集積比とシンチグラムの結果を示した．腫瘍血液の放射能集積比は，経時的に向上し，シンチグラムにおいても，マウスの左大腿部に移植した腫瘍をイメージングすることに成功した.[10] しかし，腫瘍以外に腎臓への高い放射能滞留も観察された．このような非特異的な放射能集積は，ほかのタンパク質・ペプチドを基盤とした放射性プローブにも観察され，^{111}In 標識抗腫瘍抗体では肝臓に，^{111}In 標識オクトレオチドでは，腎臓に非常に高い放射能集積が認められ，腫瘍の診断精度の低下や不要な放射線被爆を引き起こす大きな原因となっている．

RI 標識抗体フラグメントやペプチドを生体内に投与後に観察される，腎臓における非特異的放射能集積を低減する目的で，RI 標識ポリペプチドを投与時の腎臓における放射能集積の化学制御に関する研究が行われている．その1つが，Brush Border Strategy と呼ばれる手法である（Fig. 4）．この手法は，RI 標識抗体フラグメントを生体に投与し，糸

球体ろ過を受けたのち，腎尿細管細胞に取り込まれる前に，刷子縁酵素カルボキシペプチダーゼMによって，尿排泄性の高い放射性化合物を速やかに遊離させることにより，腎臓への非特異的な放射能集積を低減させるという原理に基づいている．カルボキシペプチダーゼMにより，グリシン-リジン配列が選択的に切断されること，メタヨード馬尿酸が速やかに尿排泄されることに着目して，放射性ヨウ素標識 *m*-ヨード馬尿酸のグリシン残基をリジンのαアミノ基と結合させ，さらにそのリジン残基のεアミノ基を抗体フラグメントとの結合に有効なマレイミド基に変換した，放射性ヨウ素標識HMLが設計・合成され，このHMLを用いて放射性ヨウ素標識したFabを用いた検討が行われた.[11] その結果，^{131}I-HML-Fabを腫瘍移植マウスに投与3時間後までに，[^{131}I]m-ヨード馬尿酸が尿中に速やかに排泄されることにより，腎臓への放射能集積はほとんど観察されず，腫瘍部位の明瞭なイメージングが達成されている．今後，本手法を^{99m}Tcや^{111}Inなどの金属RIに応用することにより，抗体フラグメントを基盤とした有効な腫瘍イメージングプローブの開発が期待される．

3. PET/SPECTによる脳神経疾患の分子イメージング

次に，代表的な脳神経疾患であるアルツハイマー病のPET/SPECTによる分子イメージングについて紹介する．

アルツハイマー病に特徴的な脳内病理学的変化として，βシート構造を取ったアミロイドβペプチドからなる老人斑の沈着と過剰にリン酸化されたタウタンパクからなる神経原線維変化の出現が知られている．これら病変の中でも，老人斑の沈着は，アルツハイマー病発症過程の最も初期段階から生じる病理学的変化と考えられ，臨床症状が現れる数十年前から始まることが明らかとなっている．したがって，体外からの老人斑の検出は，アルツハイマー病の早期診断につながると考えられることから，現在，アミロイドイメージングプローブを利用した老人斑のインビボ画像診断が注目されている．

老人斑アミロイドは，アルツハイマー病脳において，アミロイド前駆タンパク質（APP）からセクレターゼβとγにより切り出されたアミロイドβペプチド（Aβ40及びAβ42）の凝集，繊維化によって生成する．この老人斑を体外より画像化するために，アミロイドイメージングプローブに求められる性質として，1）生体内へ投与後に，血液脳関門を通過すること，2）老人斑に選択的に結合し，3）老人斑アミロイドに結合しない非結合分子は速やかに脳から血液へ消失することが挙げられる．老人斑アミロイドのインビボ分子イメージングは，このような条件を満たして老人斑アミロイドに特異的に結合したアミロイドイメージングプローブから放出されるガンマ線をPET/SPECT装置を用いて体外より検出し，老人斑を画像化するという原理に基づい

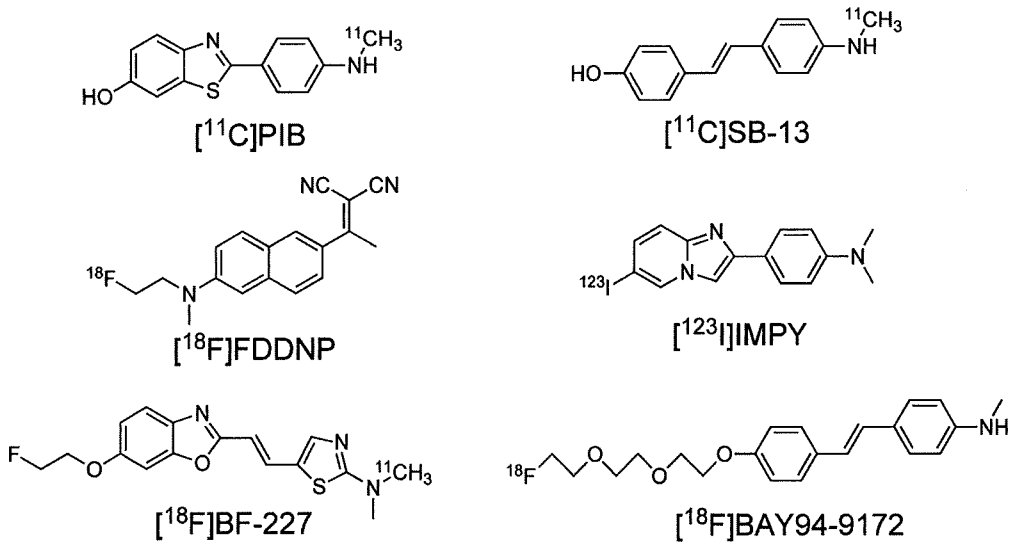

Fig. 5. Chemical Structures of β-Amyloid Imaging Probes Tested Clinically

ている．

Figure 5 には，これまでに臨床で使用されたアミロイドイメージングプローブの化学構造式を示す．[12–17] その多くが老人斑の蛍光染色試薬であるコンゴーレッド，チオフラビン T の構造を基に開発されており，^{11}C あるいは ^{18}F で標識された 5 種類の PET 用プローブ及び ^{123}I で標識された 1 種類の SPECT 用プローブが臨床評価された．PET 用プローブによる多くの臨床研究が行われ，アルツハイマー病診断におけるアミロイドイメージングの有用性が報告されてきた一方で，SPECT 診断用プローブとしては，[^{123}I] IMPY が報告されているが，脳移行後の非特異的放射能滞留が認められることから，より高性能なプローブの開発が望まれている．

現在最も多くの臨床研究が行われている [^{11}C] PIB の臨床研究の PET 撮像の結果を Fig. 6 に示した．アルツハイマー病患者の脳は，コントロールには観察されない，非常に高い放射能集積が観察され，PIB のアミロイドイメージングにより，アルツハイマー病患者と健常人との鑑別は可能であることが報告されている．[13] また，ヒトアミロイド斑には高い結合性を示す一方，マウスアミロイド斑への結合性が低いことが報告されており，[18] 最近の論文において，マウスアミロイド斑には存在せず，ヒトアミロイド斑に多く存在する N 末端がピログルタミン酸修飾されたアミロイド β42 への PIB の結合性が示唆されている．[19]

次に，われわれが開発した PET 用アミロイドイメージングプローブを紹介する．PIB の化学構造中のチアゾールをフランに変換した，フェニルベンゾフランを基本骨格とする，[^{11}C] HMBZF [5-hydroxy-2-(4-[^{11}C] methylaminophenyl) benzofuran] を設計・合成した．アルツハイマー病患者脳ホモジネートを用いた阻害実験を行った結果，阻害定数 (K_i) が 0.7 nM と PIB の 4.3 nM よりもアミロイドへの高い結合性を示した．正常マウスにおける体内放射能分布実験を行ったところ，投与初期の高い脳移行性とその後の速やかなクリアランスを示すことが明らかとなった．次に，アルツハイマー病モデルマウスに投与後，*ex vivo* オートラジオグラフィーを行った結果，野生型マウスに比べ，高い放射能集積が認められ，さらにこの放射能集積は，アミロイドの蛍光染色試薬チオフラビン S の染色位置と一致した (Fig. 7)．これらの結果より，HMBZF が PET 用アミロイドイメージングプローブとして有用であることが示された．[20]

前述のように，既報のアミロイドイメージングプローブは，その多くがコンゴーレッドやチオフラビン T から派生した化学構造であることから，われわれはアミロイドイメージングプローブとして機能する新たな分子骨格の探索研究を行ってきた．最近，インビトロにおいて，フラボノイド化合物にアミロイド β ペプチドの凝集，繊維化抑制作用があることが報告され，アミロイド β との結合性あるいは相互作用があることが考えられた．そこで，これら化合物の共通構造である，フラボン骨格をアミロイドイメージングプローブの新たな骨格に選択し，SPECT 用 RI であるヨウ素と種々の置換基を導入したフラボン誘導体を設計・合成し，アミロイドイ

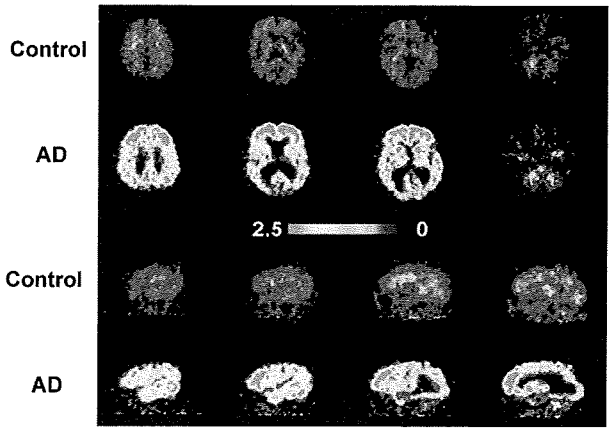

Fig. 6. [^{11}C] PIB-PET in Healty Controls and Alzheimer's Disease (AD) Patients[13]

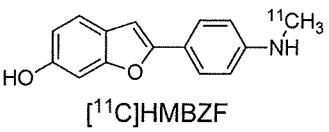

[^{11}C]HMBZF

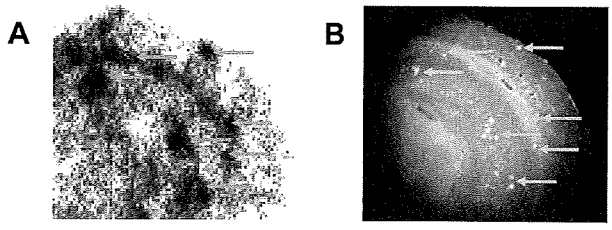

Fig. 7. *Ex vivo* Autoradiography of [^{11}C] HMBZF Using AD Model Mice (A), Thioflavin S Staining in the Same Brain Section (B)